Drug Design, Development and Therapy

Dovepress
Taylor & Francis Group

Open Access Full Text Article

ORIGINAL RESEARCH

# Integrating Clinical Multi-Omics, Machine Learning, and Molecular Docking Strategies to Reveal the Mechanism of Yiqi Huoxue Prescription in the Treatment of Ischemic Heart Failure

Jingjing Wei[1], Lijie Qiao[1], Peng Yu[2], Ying Li[3], Xingyuan Li[1], Ming Li[1], Xinfeng Zhu[1], Wenjun Wu[1], Aolong Wang[1], Yilin Zhang[1], Lanxin Li[1], Bin Li[1], Qifei Zhao[1], Rui Yu[1], Yizho Li[1], Zhengwei Dong[1], Shanshan Nie[1], Yongxia Wang[1], Xinlu Wang[1], Mingjun Zhu[1]

[1]Department of Cardiovascular Disease, The First Affiliated Hospital of Henan University of Chinese Medicine, Zhengzhou, Henan, 450000, People's Republic of China; [2]Department of Orthopedics, The First Affiliated Hospital of Henan University of Chinese Medicine, Zhengzhou, Henan, 450000, People's Republic of China; [3]Department of Basic Medical Research, Xiyuan Hospital of China Academy of Chinese Medical Sciences, Beijing, 100091, People's Republic of China

Correspondence: Mingjun Zhu; Xinlu Wang, The Department of Cardiovascular Disease, The first Affiliated Hospital of Henan University of Chinese Medicine, Zhengzhou, Henan, 450000, People's Republic of China, Email zhumingjun317@163.com; wangxinlu110@126.com



**Objective:** Ischemic heart failure (IHF) is a multifaceted syndrome associated with significant mortality and high hospitalization rates globally. Yiqi Huoxue prescription (YQHX) has been incorporated into clinical practice, showing significant therapeutic efficacy. However, to date, the pharmacological mechanisms remain vague. We combined multi-omics, machine learning, and molecular docking strategies to elucidate the mechanisms by which YQHX protects against IHF.

**Methods:** Clinically, the efficacy and safety of YQHX in improving cardiac function in IHF patients were observed. Transcriptomic, proteomic, and targeted metabolomic analyses were performed on serum samples from IHF patients and healthy individuals before and after YQHX intervention. Multi-omics association analysis integrating machine learning identified the potential mechanisms underlying YQHX's effects. Key ingredient-targets interactions were validated in vitro experiments.

**Results:** After 12 weeks of treatment, YQHX significantly decreased N-terminal pro-B-type natriuretic peptide (NT-proBNP) (MD, −1180.28; 95% CI: −2107.23 to −253.32), enhanced left ventricular ejection fraction (LVEF) (MD, 4.78; 95% CI: 2.23 to 7.32), and improved 6-minute walk distance (6MWD). No serious adverse events were observed during the study. Multi-omics integration analysis revealed that platelet activation NET formation, HIF-1 signaling pathway, TCA cycle, and glycolysis are indispensable pathways for the treatment of IHF. Machine learning has identified H3-3A, HMGB1, SOD2, ACTG1, PGAM1, FGA, LDHA, FN1, VWF, and ACO2 as critical molecular targets of YQHX treatment. Clinical research further demonstrated that YQHX treatment beneficially modulates energy metabolism, improves coagulation system functions, and ameliorates inflammatory responses in IHF. Molecular docking revealed that astragaloside I/III/IV, isoastragaloside I/II, paeoniflorin, and hydroxysafflor yellow A are likely active compounds contributing to YQHX's therapeutic effects, and these findings were further validated through in vitro experiments.

**Conclusion:** YQHX combats IHF via multi-target and multi-pathway mechanisms, including energy metabolism reprogramming, coagulation system enhancement, and immune-inflammatory response modulation, positioning it as a potential therapeutic strategy for IHF.

**Keywords:** ischemic heart failure, Yiqi Huoxue, multi-omics, machine learning, molecular docking, traditional Chinese medicine

Received: 3 March 2025
Accepted: 3 November 2025
Published: 6 November 2025

**Graphical Abstract**

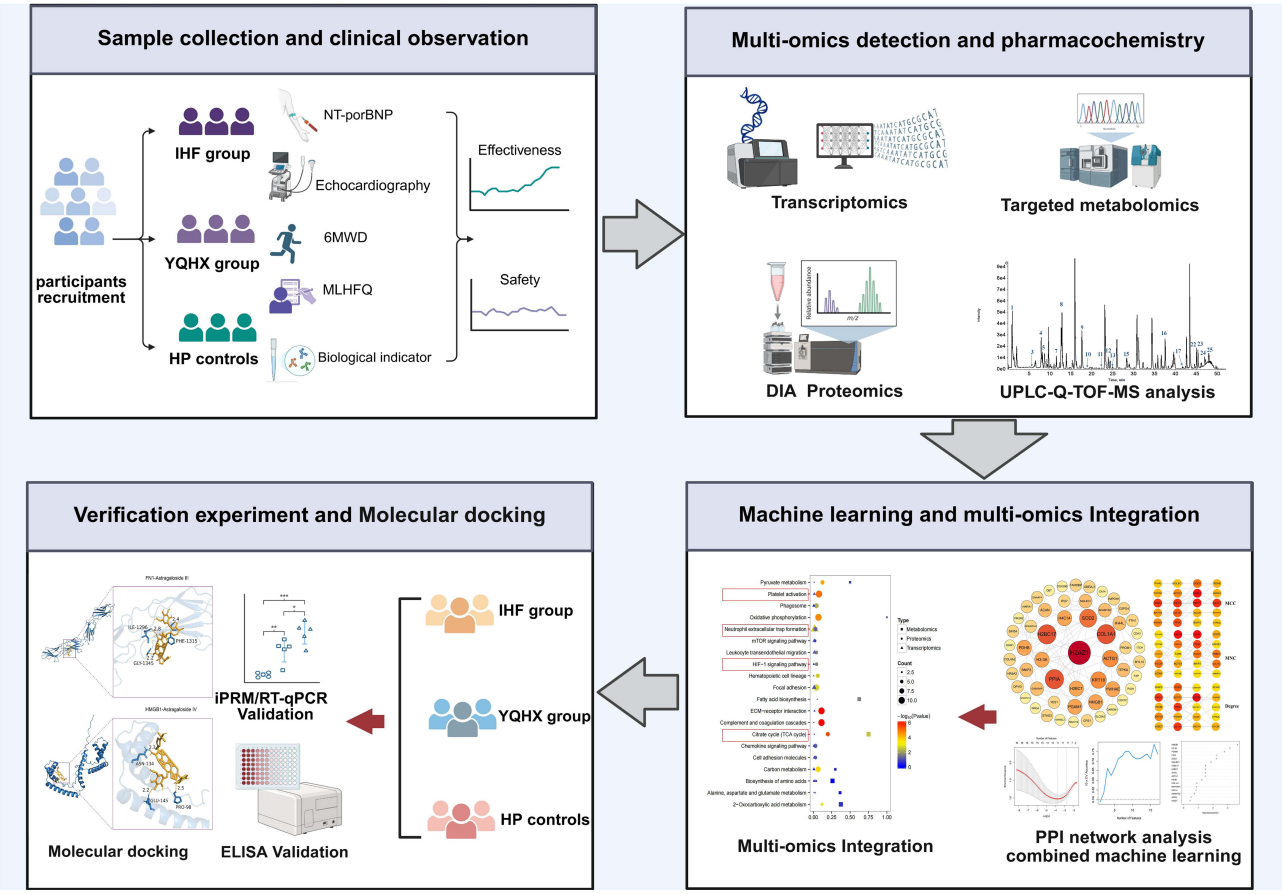


# Introduction

Heart failure (HF) remains a leading cause of morbidity and mortality worldwide, with its burden continuing to rise as populations age. A 2021 large-scale epidemiological survey reported a standardized HF prevalence of 1.10% among Chinese adults aged ≥25 years, translating to approximately 12.1 million affected individuals.[1] Nearly 3 million new cases occur annually, with patients averaging 3.3 hospitalizations per year and an annual per capita hospitalization cost of $4406.8. In the United States, HF represents the most common cause of hospitalization among older adults, imposing an estimated annual cost of $40 billion. This figure is projected to increase to nearly $69.7 billion by 2030, creating a substantial economic burden on public health.[2] Ischemic heart disease (IHD) accounts for nearly 70% of HF cases, making it the predominant etiological factor.[3] IHD increases the risk of HF by eightfold, with attributable risks of 65% in men and 48% in women.[4] Despite efforts to mitigate critical risk factors for IHD, hospitalization rates for ischemic heart failure (IHF) have remained largely unchanged and are projected to rise further. Moreover, unresolved challenges in IHF management, including incomplete symptom alleviation, adverse drug reactions, and variability in individual responses, highlight the need for better treatment strategies. Consequently, there is a pressing need to explore and develop innovative pharmacological therapies aimed at improving outcomes in IHF.

Traditional Chinese Medicine (TCM), a prominent branch of complementary medicine, has gained considerable popularity in both Asia and Western countries over recent decades, showing potential as an adjunct to existing therapies for IHF.[5] Clinically, several Chinese herbal medicines have been employed as adjunctive treatments for HF. For example, a randomized, double-blind, placebo-controlled, multicenter clinical trial involving 3119 chronic heart failure patients

showed that Qili Qiangxin capsules reduced the risk of the primary composite endpoint of HF worsening, rehospitalization, and cardiovascular death by 22%.[6] A randomized controlled trial involving 640 IHF patients across 32 tertiary hospitals revealed that Qishen Yiqi Dripping Pills significantly improved exercise tolerance in IHF with a favorable safety profile.[7] Yiqi Huoxue prescription (YQHX) is derived from the classical TCM prescription "Buyang Huanwu Decoction", as described in the Qing Dynasty medical classic Yi Lin Gai Cuo (1830 AD), and has been extensively applied in clinical cardiovascular treatments. YQHX is composed of Huangqi (Astragali Radix) 60g, Danggui (Angelicae Sinensis Radix) 20g, Chishao (Paeoniae Radix Rubra) 15g, Chuangxiong (Chuanxiong Rhizoma) 12g, Dilong (Lumbricus) 12g, Honghua (Carthami Flos) 12g, and Taoren (Persicae Semen) 12g. Our prior multi-center, double-blind clinical trial demonstrated that YQHX, when used alongside standard treatment, significantly improved cardiac function, reduced N-terminal pro-B-type natriuretic peptide (NT-proBNP) levels, enhanced exercise tolerance in IHF patients, and showed no notable adverse effects.[8] Network pharmacology and in vitro studies have revealed that YQHX attenuates myocardial fibrosis via downregulation of pro-inflammatory cytokines and modulation of the IL-17 signaling cascade.[9] In earlier research, we identified 11 key compounds from YQHX using liquid chromatography-tandem mass spectrometry (LC-MS/MS), primarily sourced from Astragali Radix, Angelicae Sinensis Radix, and Paeoniae Radix Rubra.[8] Previous studies reported that major YQHX compounds, including CID44715618, naringin, calycosin-7-O-beta-D-glucoside, and ginsenoside F1, prevent myocardial ischemia-reperfusion (I/R) injury by enhancing energy metabolism, regulating autophagy, reducing oxidative stress, and inhibiting inflammation and necrosis.[10] Fengming Tian et al discovered that YQHX active components, including adenine, guanosine, and genistein 7-O-β-D-glucoside, may influence angiogenesis through glycolytic reprogramming.[11] Nevertheless, the precise mechanisms underlying YQHX's effects on IHF require further exploration.

The integration of systems biology and molecular docking has effectively explored the synergistic mechanisms of multi-component, multi-target, and multi-pathway interactions in TCM across different diseases.[12,13] In this study, we established an integrative strategy to deeply investigate the therapeutic mechanisms of YQHX in treating IHF. Initially, we employed ultra-performance liquid chromatography coupled with quadrupole time of flight mass spectrometry (UPLC-Q-TOF-MS) to identify the compounds in YQHX, providing pharmacologically active candidate components. Subsequently, we enrolled IHF patients and healthy volunteers who met clinical research criteria and evaluated the therapeutic effects of YQHX after 12 weeks of treatment. Furthermore, transcriptomics, data-independent acquisition (DIA)-based proteomics, and targeted metabolomics studies identified differentially expressed genes, proteins, and metabolites regulated by YQHX. Machine learning techniques, including Least Absolute Shrinkage and Selection Operator (LASSO) regression, Support Vector Machine Recursive Feature Elimination (SVM-RFE), and Random Forest (RF) algorithms, were used to identify candidate biomarkers associated with YQHX treatment of IHF. To comprehensively understand the underlying mechanisms, we integrated multi-omics data using molecular docking techniques to predict the relationships between the active components and targets of YQHX. Finally, validation experiments confirmed these findings and clarified the potential targets and signaling pathways of YQHX.

# Materials and Methods

## Study Design

This clinical study was conducted in compliance with the Helsinki Declaration and the Drug Administration Law of the People's Republic of China and was performed at the First Affiliated Hospital of Henan University of Chinese Medicine from June 2022 to July 2023. The study protocol and informed consent form were approved by the Ethics Committee of the First Affiliated Hospital of Henan University of Chinese Medicine (Approval No: 2021HL-178). All participants were recruited from the cardiology outpatient clinic of the First Affiliated Hospital of Henan University of Chinese Medicine. All participants signed a written informed consent form agreeing to participate in the study and allowing their data to be publicly disclosed. This study was officially registered with the China Clinical Trial Registration Center in April 2022, under registration number ChiCTR2200058314 (https://www.chictr.org.cn/).

## Participants

Patients are eligible for inclusion if they meet the following criteria: 1) Age 40–80 years; 2) Ischemic heart failure patients meeting the 2018 Chinese guidelines for the diagnosis and treatment of heart failure and the 2022 AHA/ACC/HFSA guidelines for the management of heart failure; 3) Left ventricular ejection fraction (LVEF) ≤ 50%, as measured by echocardiography using the modified Simpson method; 4) New York Heart Association (NYHA) Class I to IV; 5) Written informed consent obtained. Healthy adults with normal physical examinations will be included. Exclusion criteria include the presence of any of the following: 1) Pulmonary embolism, acute coronary syndrome, or acute cerebrovascular disease; 2) Other heart diseases such as valvular heart disease, severe valve abnormalities, myocardial disease, congenital heart disease, or pulmonary heart disease; 3) Liver and/or kidney dysfunction, malignancies, or autoimmune diseases; 4) Psychosis or substance abuse; 5) Absolute contraindications to Traditional Chinese Medicine (TCM); 6) Pregnancy, planning for pregnancy, or breastfeeding.

## Interventions

All IHF participants received standard Western medical treatments, including diuretics, renin-angiotensin system inhibitors, β-receptor blockers, MRA aldosterone receptor antagonists, SGLT2 inhibitors, and cardiac glycosides. The specific treatment strategies were individualized based on the 2018 Chinese guidelines for the diagnosis and treatment of HF and the 2022 AHA/ACC/HFSA guidelines for the management of HF. In addition to the standard Western medical treatment, participants in the IHF group were given YQHX granules (21.6 g, twice daily; provided by Jiangyin Tianjiang Pharmaceutical Co., Jiangsu, China) orally for 12 weeks. YQHX consisted of seven natural medicinal ingredients: 60g of Astragali Radix (Gansu, China, Lot No. 231202), 20g of Angelicae Sinensis Radix (Gansu, China, Lot No. 231202), 15g of Paeoniae Radix Rubra (Guangxi, China, Lot No. 231203), 12g of Chuanxiong Rhizoma (Sichuan, China, Lot No. 240101), 12g of Lumbricus (Gansu, China, Lot No. 231203), 12g of Carthami Flos (Xinjiang, China, Lot No. 231201), and 12g of Persicae Semen (Hebei, China, Lot No. 2312081). All TCM components were supplied by The First Affiliated Hospital of Henan University of Chinese Medicine and processed into granules by Jiangyin Tianjiang Pharmaceutical Co., Ltd., utilizing modern techniques such as extraction, concentration, drying, granulation, and sealing, exclusively for clinical research (approval number: 2204317). The herbal granules were manufactured in strict compliance with the 2020 edition of the "Chinese Pharmacopoeia". The compounds in YQHX were analyzed using UPLC-Q-TOF-MS to ensure effective quality control of the preparation. The UPLC-Q-TOF/MS-determined characteristic chromatogram and information for the 25 active components in YQHX can be found in Figure S1 and Table S1, detailing the major chemical classes in YQHX, including triterpene saponins, flavonoids and flavonoid glycosides, cyanogenic glycosides, monoterpene glycosides, nucleotides, phenylpropanoids, amino acids, organic acids, and others.

## Clinical Efficacy Evaluation Index

NT-proBNP levels before and after treatment were measured using a colloidal gold test kit (Getein Biotech, Nanjing, China). LVEF, left ventricular end-diastolic dimension (LVEDD), left ventricular end-diastolic volume (LVEDV), and stroke volume (SV) were measured using a color Doppler ultrasound diagnostic device (GE Vivid E95, USA) employing the two-dimensional Simpson's method. The 6-minute walk distance (6MWD) was assessed by researchers who had completed standardized training. Patient quality of life was assessed using the Minnesota Living with Heart Failure Questionnaire (MLHFQ). Laboratory parameters included blood lipids, blood glucose, coagulation function, complete blood count, liver function, kidney function, and urine analysis. The above endpoints were measured and recorded at weeks 0 and 12 during the treatment period to evaluate the treatment's efficacy and safety.

## RNA-Seq-Based Transcriptomic Study

Fasting venous blood samples (2.5 mL) were collected from each subject in the morning using PAXgeneTM tubes (PreAnalytiX, China), gently inverted 8–10 times for thorough mixing, labeled, and gradient-frozen following the manufacturer's instructions. Total RNA was extracted from the blood samples using the PAXgene Blood miRNA Kit (PreAnalytiX, China). RNA concentration and integrity were precisely measured using an Agilent 5400 Bioanalyzer

(Agilent Technologies, USA) and a Nanodrop spectrophotometer (BioForge, China). Sequencing was performed on the Illumina NovaSeq 6000 high-throughput platform (Illumina, USA). Differentially expressed genes (DEGs) were identified using the criteria of $|\log2FC| \geq 1$ and adjusted $P < 0.05$.R packages "Clusterprofiler" and "DOSE" were used to perform GO, and KEGG enrichment analysis.

## Data-Independent-Acquisition-Based Proteomic Study

Fasting venous blood samples were collected from each participant in the morning and placed into 2 mL anticoagulant tubes containing ethylenediaminetetraacetic acid (EDTA) for centrifugation. The supernatant was centrifuged at 3000×g for 15 minutes at 4°C. The fresh supernatant was then collected into Eppendorf tubes, labeled, and stored at −80°C. Proteins were extracted and identified following the manufacturer's instructions, using the Proteominer low-abundance protein enrichment kit (Bio-Rad, USA) to deplete high-abundance proteins.[14] Protein concentration in the samples was measured using the Bradford protein assay kit (Biyuntian, China). After desalting the enzymolysis peptides, the samples were analyzed using LC-MS/MS.[15] A detailed description of the DIA-based proteomic study methodology can be found in Table S2. The DEPs were selected based on criteria of FC > 1.5 or FC < 0.67 and $P < 0.05$.

## Targeted Metabolomics Study

Fasting venous blood samples were collected from each participant in the morning and placed into 2 mL anticoagulant tubes containing EDTA for centrifugation. The supernatant was centrifuged at 3000×g for 10 minutes at 4°C. The fresh supernatant was then collected into Eppendorf tubes, labeled, and stored at −80°C. Target metabolites were extracted following the manufacturer's protocol. An ultra-high performance liquid chromatography coupled with tandem mass spectrometry (UHPLC-MS/MS) system (ExionLC™ AD UHPLC-QTRAP 6500+, AB SCIEX Corp., Boston, MA, USA) was employed to quantify the metabolites. Detailed procedures for targeted metabolomics are outlined in Table S3. The data were processed using the metabolomics software metaX, followed by principal component analysis (PCA) and partial least squares discriminant analysis (PLS-DA) to determine the variable importance in projection (VIP) of each metabolite. The statistical significance between the two groups for each metabolite was assessed using a *t*-test, and FC between the groups was also calculated. Differentially expressed metabolites (DMs) were identified based on the criteria of upregulated metabolites with FC > 1.2, downregulated metabolites with FC < 0.833, and VIP > 1.

## Protein-Protein Interaction (PPI) Network Construction and Screening Candidate Biomarkers

Mapping DEGs/DEPs to the STRING database (https://string-db.org/), with a filter criterion of a minimum required interaction score of 0.4, removing unconnected nodes to establish the PPI network. After downloading the PPI analysis results, we input them into the Cytoscape software (version 3.10.2) for further optimization. Network topology and node centrality analyses were performed using the cytoHubba plugin. We employed the Maximal Clique Centrality (MCC), Neighborhood Component Centrality (MNC), and Degree algorithms to identify the top 15 signature genes/ proteins in the core module.

Next, we employed three complementary machine learning algorithms (LASSO, SVM-RFE, and RF), implemented through the R packages *glmnet, e1071*, and *randomForest*, respectively, to identify optimal signature genes/proteins. This integrated strategy leverages distinct algorithmic strengths to balance sparsity, high-dimensional feature ranking, and non-linear interaction detection: LASSO applies L1-regularization to perform feature shrinkage and variable selection, effectively preventing overfitting while retaining the most predictive features;[16] SVM-RFE employs margin-based iterative feature elimination, demonstrating particular efficacy in high-dimensional omics data optimization;[17] RF utilizes ensemble decision trees with bootstrap aggregation to capture complex feature interactions while ranking variables by their node impurity reduction importance.[18] The top-ranked biomarkers from each algorithm were intersected to identify candidate biomarkers associated with YQHX treatment. A receiver operating characteristic (ROC) curve was subsequently plotted.

## Joint Analysis of Transcriptomics, Proteomics, and Metabolomics

Using the ClueGO and CluePedia plugins of Cytoscape 3.10.2, we analyzed the KEGG pathways and Gene Ontology (GO) enrichment of potential targets based on DEGs/DEPs identified in the YQHX treatment for IHF. This was done to clarify the key biological processes regulated by YQHX, with pathway analysis set to a significance level of $P \leq 0.05$. DEGs, DEPs, and DMs related to YQHX treatment for IHF were mapped to the KEGG pathway database using the "Pathview" package in R, allowing us to obtain the shared pathway information. KEGG Mapper was used to highlight the nodes of DEGs, DEPs, and DMs in the enriched pathways, with each node displayed in different colors.

## iPRM Quantitative Proteomic Analysis

Using Intelligent Parallel Reaction Monitoring (iPRM) technology, 14 target proteins were identified and quantitatively validated. Samples were retrieved from storage at −80°C and processed for protein extraction and quantification using the previously described proteomics protocol. After quality control validation, enzymatic digestion and desalting were performed. Peptide information was acquired in DIA mode, generating raw mass spectrometry data files (.raw). Spectronaut software was used to identify and quantify proteins, selecting unique peptides corresponding to the differential target proteins. The chromatographic method remained consistent with the DIA data acquisition approach. The iPRM list was imported into the mass spectrometry acquisition method settings file and edited to establish the iPRM acquisition method. The acquisition mode utilized was Full MS-PRM.

## Preparation of Drug-Containing Serum

Male SD rats (200–220 g) were purchased from Beijing Vital River Laboratory Animal Technology Co., Ltd. (Production License SCXK2024-0001). All animal procedures were approved by the Animal Ethics Committee of Henan University of Chinese Medicine (IACUC-202504015). YQHX-containing serum and blank serum were prepared according to an established protocol. Rats (8 weeks old) were divided into two groups (n=6/group): blank serum group (received distilled water volume-matched to YQHX group) and YQHX serum group (17.45 g/kg/day). YQHX was administered by gavage for 7 consecutive days. Blood samples were collected from the abdominal aorta under anesthesia 2 h after the last administration, allowed to clot for 2 h at room temperature, and centrifuged at 3000 rpm for 15 mins. The supernatant was inactivated at 56°C for 30 mins, sterilized by filtration, and stored at −80°C.

## Cell Culture and Treatment

H9c2 cells (Shanghai Institute of Biochemistry and Cell Biology, Chinese Academy of Sciences) were cultured in DMEM supplemented with 10% fetal bovine serum (FBS) and 1% penicillin/streptomycin at 37°C under 5% $CO_2$. Cells in logarithmic growth phase were seeded in 96-well plates at $5\times10^3$ cells/well. After 12 h, hypoxia injury models were established using cobalt chloride ($CoCl_2$; Sigma-Aldrich Co., Ltd., C2911) as a chemical inducer. Culture medium was replaced with complete medium containing $CoCl_2$ (0, 25, 50, 100, 200, or 400 μM) for 24 h to determine optimal modeling concentration. Cell viability was assessed by CCK-8 assay measuring optical density (OD) at 450 nm. Based on preliminary results, drug interventions were tested post-hypoxia: YQHX serum (0%, 1.25%, 2.5%, 5%, 10%, 15%, 20%) and Astragaloside IV (AS-IV; Shanghai yuanye Bio-Technology Co., Ltd., B20564, HPLC ≥98%; 0, 5, 10, 20, 40, 80 μM). Experimental groups included: Control, Model (hypoxia), YQHX, and AS-IV.

## Measurement of Cellular ATP Content and CK Activity

ATP levels were quantified using a chemiluminescence assay kit (Wuhan Elabscience Biotechnology Co., Ltd., E-BC-F002) according to manufacturer instructions. Creatine kinase (CK) activity was measured with a colorimetric kit (Wuhan Elabscience Biotechnology Co., Ltd., E-BC-K558-M) following standardized protocols.

## Detection of Apoptosis Rate

Cell apoptosis was analyzed using an Annexin V-FITC/PI kit (Wuhan Elabscience Biotechnology Co., Ltd., E-CK-A217) . Cells from each group were washed twice with PBS, resuspended in 500 μL binding buffer ($2\times10^5$ cells), and stained

with 5 μL Annexin V-FITC plus 10 μL propidium iodide (PI) for 5 min at room temperature in the dark. Apoptosis rates were determined by flow cytometry (POWCLIN SFLO, China).

## Western Blot Analysis

Total protein was extracted using RIPA lysis buffer (Shanghai solarbio Bioscience & Technology Co., Ltd., R0010) containing PMSF. Equal protein amounts were separated by 10% SDS-PAGE and transferred to PVDF membranes. After blocking with 5% BSA (Shanghai Beyotime Biotechnology Co., Ltd., ST023) for 1 h at room temperature, membranes were incubated overnight at 4°C with primary antibodies: LDHA (GeneTex Co., Ltd., GTX101416), FN1 (GeneTex Co., Ltd., GTX112794), ACO2 (Affinity Biologicals Co., Ltd., DF12346), and β-actin (Proteintech Group Co., Ltd., 20,536-1-AP). Following three 10-min TBST washes, membranes were incubated with HRP-conjugated secondary antibody (Shanghai solarbio Bioscience & Technology Co., Ltd., A0208) for 1 h at room temperature. Protein bands were visualized using ECL reagent (Shanghai solarbio Bioscience & Technology Co., Ltd., P0018) on a chemiluminescence imaging system (Monadbiotech QuickChemi 5200, China). Band intensities were quantified with ImageJ software and normalized to β-actin.

## Real-Time Quantitative Polymerase Chain Reaction (RT-qPCR)

The RT-qPCR was conducted using BlazeTaq™ SYBR® Green qPCR mix 2.0 (GeneCopoeia Green, USA), with primer sequences listed in Table S4. A housekeeping gene (β-actin) was used as an endogenous control for normalization. The Relative mRNA expression was calculated using the $2^{-\Delta\Delta Ct}$ method in a triplicated manner.

## ELISA Assay

Fasting venous blood samples were drawn in the morning and collected into 2 mL anticoagulant tubes containing EDTA for centrifugation. Samples were centrifuged at 3000×g for 15 minutes at 4°C, and the resulting plasma supernatant was carefully aspirated into polypropylene tubes. Plasma aliquots were stored at −80°C until analysis. Plasma levels of ATP (Beijing Solarbio Science & Technology Co., Ltd., BC0305), Acetyl-CoA (Wuhan Elabscience Biotechnology Co., Ltd., E-EL-0125), PGI2 (Wuhan Elabscience Biotechnology Co., Ltd., E-EL-0022), TXA2 (Wuhan Elabscience Biotechnology Co., Ltd., E-EL-0057), TAT (Wuhan Elabscience Biotechnology Co., Ltd., E-EL-H1788), TNF-α (Wuhan Elabscience Biotechnology Co., Ltd., E-EL-H0109), IL-1β (Wuhan Elabscience Biotechnology Co., Ltd., E-EL-H0149), IL-6 (Wuhan Elabscience Biotechnology Co., Ltd., E-EL-H6156), MPO (Wuhan Elabscience Biotechnology Co., Ltd., E-BC-K074-M), cell-free DNA (cfDNA, Beijing Solarbio Science & Technology Co., Ltd., D1810), Cit H3 (Wuhan Colorful Gene Biological Technology Co., Ltd., ELK0742), and NE (Wuhan Elabscience Biotechnology Co., Ltd., E-EL-H1946) were quantified using ELISA kits, following the manufacturer's instructions. The concentrations of TNF-α, IL-1β, and IL-6 in H9c2 cell supernatants were quantified using commercial ELISA kits (Wuhan Elabscience Biotechnology Co., Ltd., E-EL-R2856, E-EL-R0012, E-EL-R0015) according to the manufacturer's protocol following centrifugation.

## Molecular Docking

First, the three-dimensional structure of the target protein receptor gene was obtained from the PDB database (http://www.rcsb.org/) and the UniProt database (https://www.uniprot.org/). Next, the core YQHX compound, identified through UPLC-Q-TOF/MS, was retrieved as a two-dimensional structure from the PubChem database (https://pubchem.ncbi.nlm.nih.gov/) and converted into a three-dimensional structure using Chem3D software. Finally, the receptor-ligand binding affinity was calculated using the docking model with AutoDock Vina 1.2.3. An affinity of $\leq -5.0$ kcal/mol was indicative of strong receptor-ligand interactions. The docking results were visualized using PyMOL 2.6.0 and Discovery Studio 2016.

## Statistical Analysis

Biological data were analyzed using GraphPad Prism version 9.0 (GraphPad Software Inc., CA, USA). Frequency counts and percentages summarized categorical variables, while means and standard deviations (SDs) represented continuous variables. The generalized estimating equation (GEE) model assessed differences in clinical outcomes between baseline and follow-up. One-way analysis of variance (ANOVA) compared group data. A $P$ -value below 0.05 indicated statistical significance.

# Results

## Demographic Factors and Baseline Characteristics

From June 2022 to July 2023, this study enrolled 40 eligible IHF patients, sourced from the First Affiliated Hospital of Henan University of Chinese Medicine. A healthy control group (HP) comprising 20 participants was simultaneously recruited from the Health Examination Center of Henan University of Chinese Medicine. Table 1 provides an overview of the baseline demographic and biochemical characteristics. Both groups were comparable in terms of age, sex, BMI, heart rate, and diastolic blood pressure at study initiation, with all participants belonging to the Han ethnicity. Interestingly, TC and LDL-C levels in the healthy control group were higher than those in the IHF patients, even though elevated LDL and TC are well-known risk factors for cardiovascular disease. However, the majority of these levels in the healthy control group remained within the normal range, with LDL <3.4 mmol/L (SUR method) and TC <5.2 mmol/L (COD-POD method). This variation could be explained by the older age of the participants (predominantly between 60 and 70 years) and the possible implementation of lipid-lowering therapies in the IHF group.

## YQHX Can Improve Heart Function and Quality of Life

Our GEE analysis revealed significant improvements in NT-proBNP levels and MLHFQ scores during the follow-up period. After 12 weeks of standard Western medical treatment combined with YQHX granules, NT-proBNP levels significantly decreased [mean difference (MD): −1180.28, 95% CI: −2107.23 to −253.32; P = 0.013], and MLHFQ scores showed marked improvement (MD: −16.4, 95% CI: −20.17 to −12.63; P < 0.001) compared to baseline values (Table 2). Furthermore, LVEF and 6MWD significantly improved after 12 weeks of standard Western medical treatment combined with YQHX granules. These enhancements were significant, with LVEF increasing by (MD: 4.78, 95% CI: 2.23 to 7.32; $P < 0.001$) and 6MWD by (MD: 33.53, 95% CI: 20.03 to 47.03; $P < 0.001$). Moreover, there was a tendency for improvement in LVEDD, LVEDV, and SV levels following treatment with the YQHX, but these changes did not reach statistical significance.

**Table 1** Baseline Demographic and Biochemical Characteristics

| | **Ischemia Heart Failure (n=40)** | **HP (n=20)** |
|---|---|---|
| Age, years | 67.68(7.85) | 64.95(3.18) |
| Female, n (%) | 6(15.00%) | 7(35.00%) |
| The Han nationality, n (%) | 40(100.00%) | 20(100.00%) |
| Seated SBP, mmHg | 133.75(21.89) | 118.55(17.80) |
| Seated DBP, mmHg | 74.83(14.36) | 74.7(10.56) |
| BMI, $kg/cm^2$ | 24.15(3.77) | 23.78(3.65) |
| HR, beat per minute | 72.08(13.92) | 67.05(8.00) |
| Biochemical profile | | |
| TC, mmol/L | 3.72(0.98) | 4.42(0.64) |
| TG, mmol/L | 1.39(0.58) | 1.10(0.35) |
| HDL-C, mmol/L | 1.20(0.27) | 1.29(0.20) |
| LDL-C, mmol/L | 2.12(0.72) | 2.95(0.53) |
| GLU, mmol/L | 5.80(0.95) | 5.04(0.48) |
| PT, s | 12.27(1.26) | 10.74(0.55) |
| APTT, s | 28.25(3.55) | 31.69(2.73) |
| TT, s | 15.36(1.89) | 15.31(0.89) |
| FIB, g/L | 3.20(0.88) | 3.32(0.55) |

**Notes**: Data are n (%) or mean (SD).

**Abbreviations**: SBP, systolic blood pressure; DBP, diastolic blood pressure; BMI, body mass index; HR, heart rate; TC, total cholesterol; TG, triglycerides; HDL-C, high-density lipoprotein cholesterol; LDL-C, low-density lipoprotein cholesterol; HDL high-density lipoprotein; GLU, glucose; PT, prothrombin time; APTT, activated partial thromboplastin time; TT, thrombin time; FIB, fibrinogen.

**Table 2** GEE Model Analysis Results for Cardiac Function Parameters and MLHFQ Scores Following 12 Weeks of Treatment with the Yiqi Huoxue Formula

| | Baseline (n=40) | Post-Treatment (n=40) | GEE Model | |
|---|---|---|---|---|
| | | | MD (95% CI) | *p*-value |
| NT-proBNP (pg/mL) | 2396.58(3433.32) | 1216.30(2184.34) | −1180.28 (−2107.23, −253.32) | 0.013 |
| LVEF (%) | 41.00(6.35) | 45.78(9.44) | 4.78 (2.23, 7.32) | <0.001 |
| LVEDD (mm) | 57.73(6.77) | 56.38(6.77) | −1.35 (−3.21, 0.51) | 0.156 |
| LVEDV (mL) | 143.41(62.81) | 133.08(51.49) | −10.34 (−23.08, 2.41) | 0.112 |
| SV (mL) | 58.04(22.70) | 61.08(23.45) | 3.04 (−3.49, 9.56) | 0.362 |
| 6MWD (m) | 371.37(77.22) | 404.90(85.62) | 33.53(20.03, 47.03) | < 0.001 |
| MLHFQ | 47.48(15.95) | 31.08(15.86) | −16.4(−20.17, −12.63) | < 0.001 |

**Notes**: Data are mean (SD).

**Abbreviations**: GEE, generalized estimating equation; MD, mean difference CI confidence interval; NT-proBNP, N-terminal pro-B-type natriuretic peptide; LVEF, left ventricular ejection fraction; LVEDD, left ventricular end-diastolic diameter; LVEDV, left ventricular end-diastolic volume; SV, stroke volume; 6 MWD, 6-minute walking distance; MLHFQ, Minnesota living with heart failure questionnaire.

## Drug Safety

All participants underwent laboratory evaluations, including complete blood count, liver function, renal function, urinalysis, and coagulation function, before and after treatment with YQHX. Our results indicated no statistically significant differences in the incidence of laboratory abnormalities in the IHF group during treatment with YQHX ($P > 0.05$) (Table S5). Notably, two patients reported mild gastrointestinal discomfort after taking the medication during the treatment period, which was tolerable. No drug-related adverse events were observed in any patients during the follow-up period. We preliminarily conclude that combining YQHX with standard Western therapy appears to be safe. These cases were meticulously documented and reported.

## Transcriptomics Identified the Genes and Pathways Related to the Effect of YQHX Against IHF

To further investigate the potential mechanisms underlying YQHX treatment for IHF, transcriptomic data from blood samples of the HP, IHF, and YQHX groups were obtained using the Illumina high-throughput sequencing platform. PCA demonstrated distinct separations among the HP, IHF, and YQHX groups (Figure 1A). The DESeq2 software was used for intergroup analysis of DEGs. The IHF vs HP group and YQHX vs IHF group obtained a total of 656 DEGs. In the IHF vs HP comparison, 318 DEGs were identified, comprising 115 upregulated and 203 downregulated genes. After YQHX treatment, 338 DEGs were identified in the YQHX vs IHF comparison, including 95 upregulated and 243 downregulated genes (Figure 1B). Intersection analysis revealed 31 overlapping DEGs between the IHF vs HP and YQHX vs IHF comparisons (Figure 1C), with 31 inversely expressed genes (Figure 1D). YQHX normalized gene expression in 9.75% of IHF patients. Pathway enrichment analysis of DEGs provides insights into key pathways involved in disease progression and therapeutic mechanisms. KEGG pathway analysis was conducted using cluster Profiler (version 4.12.0) to enrich DEGs in the IHF vs HP and YQHX vs IHF comparisons. The analysis identified 17 pathways enriched with DEGs common to both comparisons (Figure 1E), associated with immune (neutrophil extracellular trap formation, Fc gamma R-mediated phagocytosis, NF-kappa B signaling pathway, Leukocyte transendothelial migration, Chemokine, Autophagy, mTOR signaling pathway, HIF-1 signaling pathway), hematological (Platelet activation), cellular communication (cell adhesion molecules, focal adhesion), and energy metabolism (TCA cycle, Glycolysis), primarily related to immune-inflammatory responses.

## Key Genes Discovery

The PPI network of YQHX-related DEGs in IHF, constructed and optimized using Cytoscape based on String data, contains 55 nodes and 74 edges (Figure S2A). Using the CytoHubba plugin, the MCC, MNC, and Degree algorithms identified the top 20 nodes of the key network. Node color intensity indicates value magnitude, with darker colors representing higher values

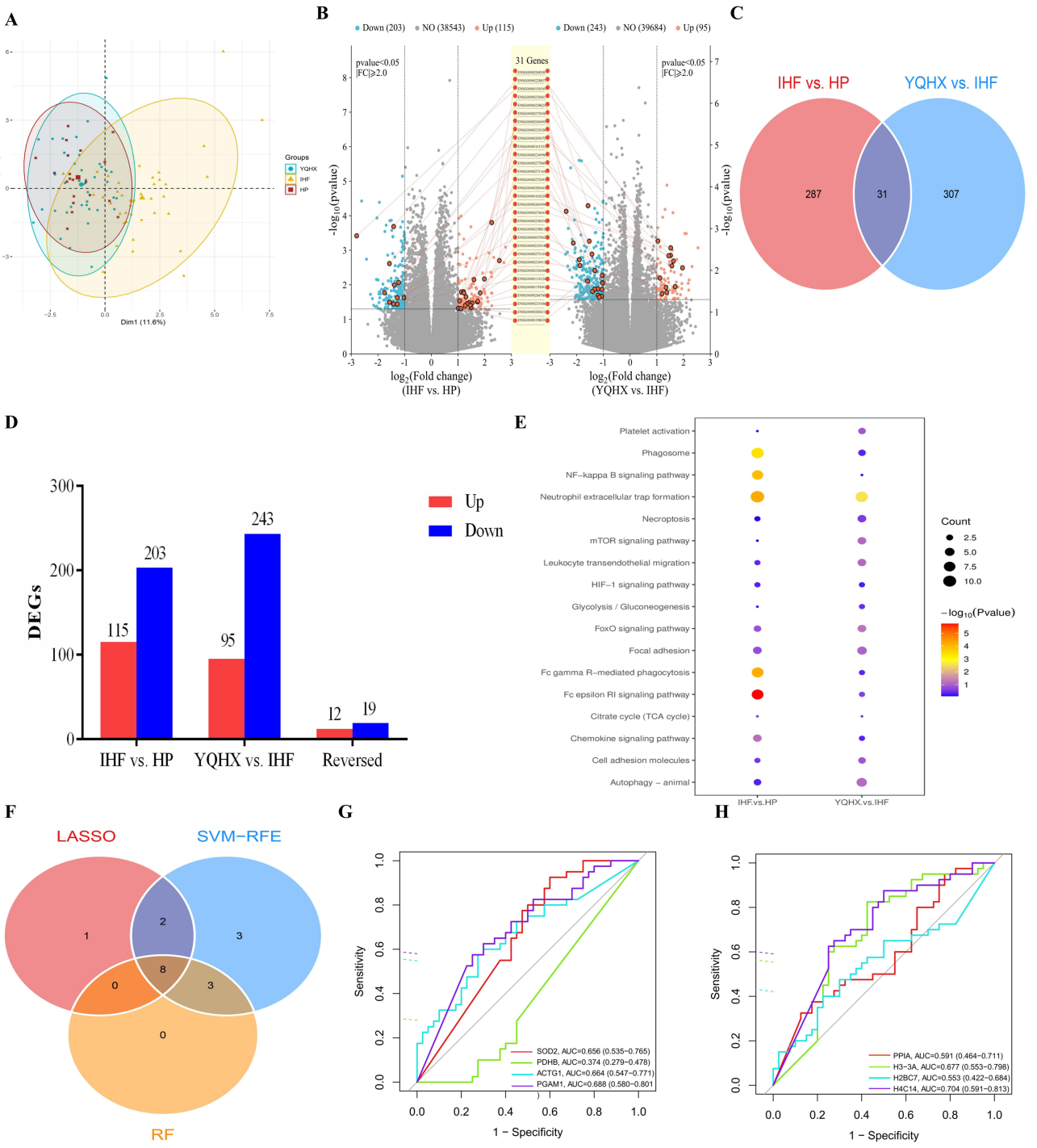


**Figure 1** Transcriptomics identified key genes and pathways related to the effect of YQHX against IHF. (**A**) Classification results of HP, IHF, and YQHX groups based on PCA score plot. (**B**) The volcano plots of DEGs. (**C**) Overlaps between DEGs of the two groups. (**D**) The distributions of DEGs for two groups and reversed DEGs. (**E**) Pathways enriched with DEGs in IHF vs HP group and YQHX vs IHF group. (**F**) Venn diagram of the intersection of signature genes obtained by the three algorithms. (**G**) ROC curve of SOD2, PDHB, ACTG1, and PGAM1. (**H**) ROC curve of PPIA, H3-3A, H2BC7, and HMGB1.

**Abbreviations**: HP, healthy people; IHF, ischemic heart failure; LASSO, Least Absolute Shrinkage and Selection Operator; RF, random forest; SVM-RFE; support vector machine recursive feature elimination; YQHX, Yiqi Huoxue prescription.

(Figure S2B). The MCC, MNC, and Degree algorithms collectively identified 17 DEGs with high centrality and betweenness. Machine learning approaches were applied to assess the potential of these 17 DEGs as candidate biomarkers for YQHX therapy in IHF. The LASSO algorithm (Figure S2C) identified 11 DEGs with minimal deviation in a binomial distribution

model, designating them as signature genes. Using 10-fold cross-validation, the SVM-RFE algorithm identified 16 signature genes with the highest accuracy (Figure S2D). The RF algorithm identified 11 DEGs with the highest contributions, categorizing them as signature genes (Figure S2E). A Venn diagram illustrated the intersection of signature genes identified by the three algorithms, revealing 8 candidate biomarkers (Figure 1F). ROC analysis indicated that H3-3A, HMGB1, SOD2, ACTG1, and PGAM1 exhibited AUC values >0.65, specifically 0.677, 0.704, 0.656, 0.664, and 0.688 (Figure 1G and H). Post-YQHX treatment, the expression levels of these five candidate biomarkers significantly reverted toward those of the healthy group, suggesting diagnostic potential and reliability. These key genes are likely critical therapeutic targets for YQHX in the treatment of IHF (Table S6).

## Proteomics Identified the Protein and Pathways Related to the Effect of YQHX Against IHF

To uncover the proteomic characteristics of IHF patients, DIA approach was employed to analyze the proteomic variations between IHF and HP controls. PLS-DA results indicated that samples from different groups were dispersed, while those within the same group clustered together (Figure 2A). Analysis revealed 211 DEPs between the IHF and HP groups, with 100 upregulated and 111 downregulated. Following YQHX treatment, 235 DEPs were detected in the YQHX group versus the IHF group, with 162 upregulated and 73 downregulated (Figure 2B). Cross-analysis identified 62 overlapping DEPs (Figure 2C), of which 59 proteins exhibited reversed expression between the IHF vs HP and YQHX vs IHF groups (Figure 2D). Furthermore, in both groups, 20 pathways enriched by DEPs were identified, many of which are associated with coagulation function and energy metabolism, such as platelet activation, complement and coagulation cascades, hematopoietic cell lineage, TCA cycle, pyruvate metabolism, and Glycolysis (Figure 2E). Following YQHX treatment, 27.96% of the proteins in IHF patients exhibited a trend toward normal expression.

## Key Proteins Discovery

The PPI network of proteins associated with YQHX treatment for IHF was constructed using Cytoscape, as shown in Figure S3A, consisting of 103 nodes and 240 edges. The key networks of the top 20 nodes were identified using the MCC, MNC, and Degree algorithms in the CytoHubba plugin, as shown in Figure S3B. Through the intersection of results from the three algorithms, 16 DEPs with high centrality and betweenness were selected. Additionally, LASSO, SVM-RFE, and RF machine learning algorithms were employed to identify 10, 14, and 7 signature proteins, respectively (Figure S3C-E). The intersection of key proteins identified by the three algorithms is presented in a Venn diagram, revealing candidate biomarkers FGA, ITGB3, FN1, VWF, and ACO2 (Figure 2F). The ROC analysis revealed AUC values of 0.972, 0.723, 0.784, 0.804, and 0.738 for FGA, ITGB3, FN1, VWF, and ACO2, respectively (Figure 2G). After YQHX treatment, the expression of these key proteins tended to return to normal (Table S7). These findings emphasize the importance of the candidate biomarkers in evaluating the accuracy and reliability of YQHX treatment for IHF.

## QSC Altered the Plasma Metabolome

To further identify the endogenous differential metabolites in IHF patients following YQHX intervention, targeted metabolite identification, and quantification were performed on blood samples from the HP, IHF, and YQHX groups using the multiple reaction monitoring approach. This study identified a total of 299 metabolites, classified into 26 categories, predominantly organic acids (11.71%), bile acids (8.70%), benzenoids (8.03%), carbohydrates (6.69%), indoles (4.01%), short-chain fatty acids (4.01%), nucleosides, nucleotides, and analogues (3.01%), phenylpropionic acids (1.67%), pyridines (1.34%), quinolines (1.00%), and fatty amides (0.67%), as shown in Figure 3A. PLS-DA model was used to establish a relationship between metabolite expression levels and sample groups, showing clear differences between the HP, IHF, and YQHX groups (Figure 3B). 150 endogenous DMs were identified in plasma, including 73 DMs between the IHF and HP groups, 77 DMs between the YQHX and IHF groups (Figure 3C), and 26 common regulated DMs (Figure 3D). Additionally, 22 DMs were found to be oppositely regulated after YQHX intervention (Figure 3E). Functional enrichment analysis (Figure 3F) revealed that the TCA cycle, pyruvate metabolism, and fatty acid biosynthesis were the three main pathways regulated by YQHX in the treatment of IHF. Violin plots revealed that seven energy

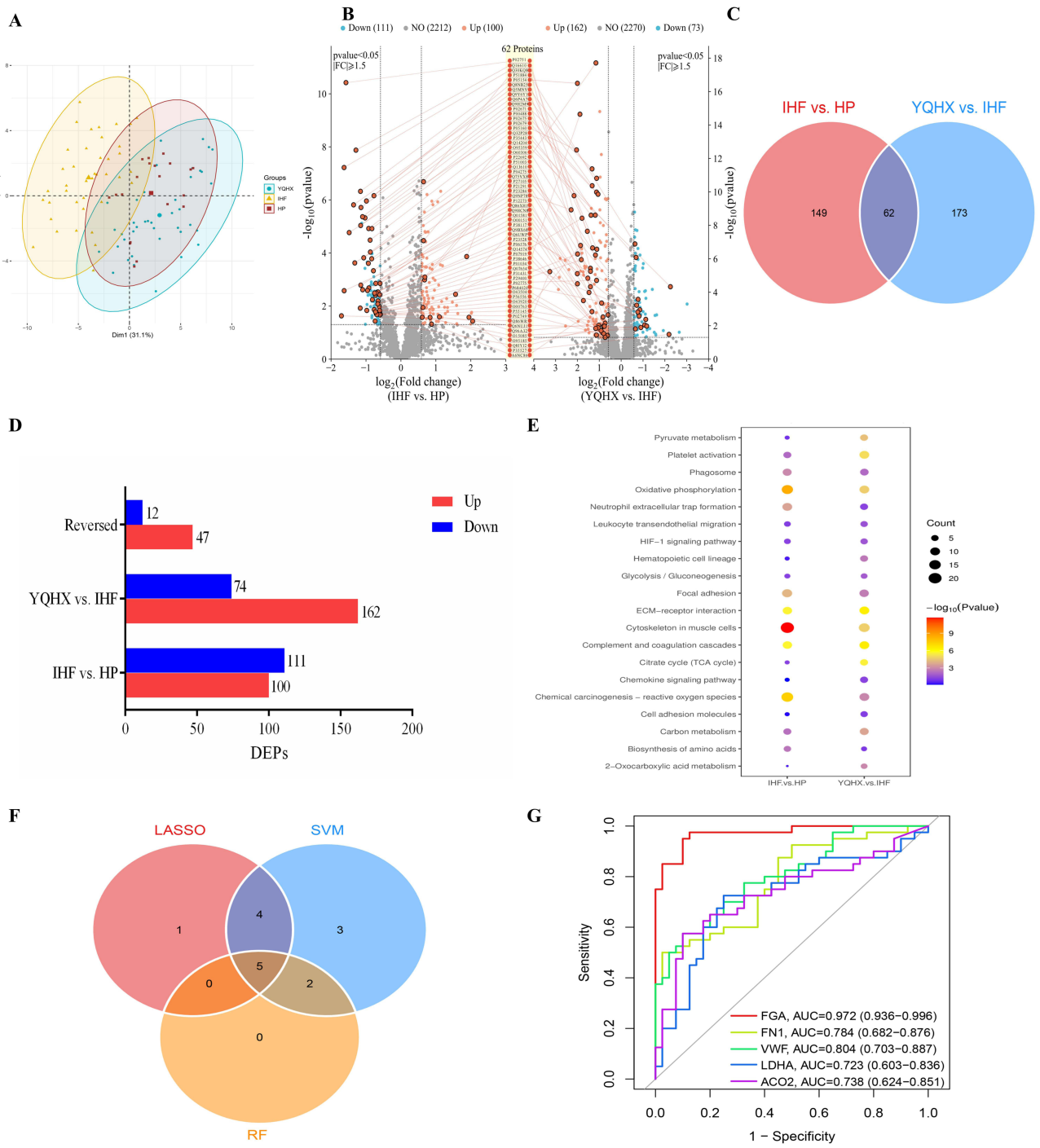


**Figure 2** Proteomics identified key proteins and pathways related to the effect of YQHX against IHF. (**A**) PLS-DA score plot of the HP, IHF, and YQHX groups. (**B**) The volcano plots of DEPs. (**C**) Overlaps between DEPs of the two groups. (**D**) The distributions of DEPs in two groups and reversed DEPs. (**E**) Pathways enriched with DEPs in IHF vs HP group and YQHX vs IHF group. (**F**) Venn diagram of the intersection of feature proteins obtained by the three algorithms. (**G**) ROC curve of FGA, ITGB3, FN1, VWF, and ACO2.

metabolism-related endogenous metabolites (citric acid, isocitrate, fumaric acid, succinic acid, L-malate, cis-aconitic acid, and L-lactic acid) were significantly elevated in the IHF group. Following 12-week YQHX treatment, these differential metabolites showed normalization trends, while pyruvic acid remained unchanged pre- and post-intervention (Figure S4).

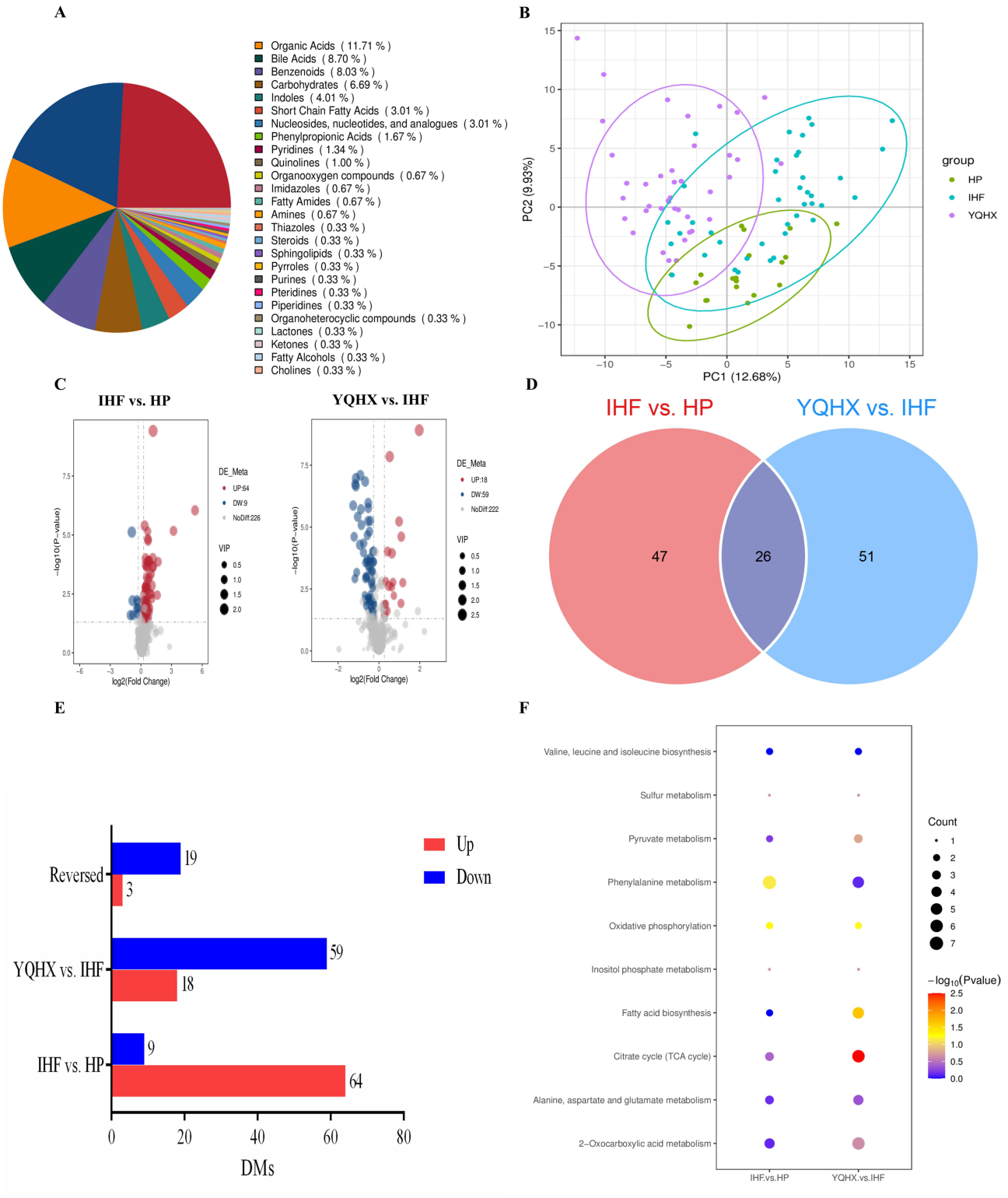


**Figure 3** Endogenous DMs and pathway enrichment analysis of serum. (**A**) Pie chart of identified metabolites. (**B**) PLS-DA score plot of the HP, IHF, and YQHX groups. (**C**) Volcanic map of reverse regulation of DMs. (**D**) Venn diagram of DMs. (**E**) The statistics of up-regulated and down-regulated DMs. (**F**) KEGG metabolic pathways enriched with DMs in IHF vs HP group and YQHX vs IHF group.


https://doi.org/10.2147/DDDT.S525675

## Integrated Analysis of DEGs, DEPs, and DMs

By integrating transcriptomic, proteomic, and metabolomic data, we aim to identify the targets and mechanisms of action of YQHX treatment. DEGs, DEPs, and DMs related to YQHX treatment in IHF were mapped to the KEGG pathway database to obtain their shared pathway information and identify the major biochemical and signaling pathways. The results indicated that the pathways enriched with the most DEGs, DEPs, and DMs were platelet activation, neutrophil extracellular trap (NET) formation, HIF-1 signaling pathway, TCA cycle, Pyruvate metabolism, and Glycolysis (Figure 4A), with candidate biomarkers occupying key positions in these pathways. Furthermore, we observed that in IHF, DEGs, DEPs in the HIF-1 signaling pathway, glycolysis, and NET formation were predominantly upregulated, while those in Platelet activation and TCA cycle were mostly downregulated. DMs in the TCA cycle were upregulated, but this pattern was reversed after YQHX treatment. We hypothesize that the mechanism of action of YQHX involves the regulation of the HIF-1 signaling pathway, which influences metabolic reprogramming, improves the coagulation system, and modulates immune-inflammatory responses, such as NET formation.

## Integrated Transcriptomic and Proteomic Analysis Revealed the Key Biological Process Regulated by YQHX

To further explore the potential mechanisms of YQHX in IHF, we performed detailed analyses of biological processes from GO analysis and KEGG pathway enrichment based on RNA-seq and proteomic results using ClueGO and CluePedia, with a significance threshold of $p < 0.05$. The top biological processes identified in the GO analysis included ATP metabolic process (GO:0046034), blood coagulation (GO:0007596), regulation of ERK1 and ERK2 cascade (GO:0070372), cellular respiration (GO:0045333), ATP-dependent protein folding chaperone (GO:0140662), fibrin clot formation (GO:0072378), and tricarboxylic acid cycle (GO:0140662), indicating that YQHX treatment of IHF primarily involves biological processes related to energy metabolism and coagulation responses (Figure 4B). KEGG enrichment analysis revealed that the pathways with significant influence included the TCA cycle, pyruvate metabolism, NET formation, platelet activation, complement and coagulation cascades, HIF-1 signaling pathway, oxidative phosphorylation, and ECM-receptor interaction (Figure 4C).

## Effect of YQHX on Energy Metabolism in Patients with IHF

Acetyl-CoA plays a central role in the energy supply chain, linking various metabolic pathways and providing substrates for the TCA cycle, while ATP, the final product of energy metabolism, serves as the direct energy source for cardiomyocytes. We evaluated the serum levels of ATP and Acetyl-CoA in the HP, IHF, and YQHX groups, randomly selecting blood samples from 10 patients in each group. Compared to the HP control group, serum ATP levels were significantly lower in the IHF group. Compared to the HP control group, serum ATP levels were significantly lower in the IHF group, but they significantly increased following YQHX treatment ($P< 0.05$, Figure 5A). Compared to the HP control group, acetyl-CoA levels showed a decreasing trend, with no significant change following YQHX treatment (Figure 5B).

## Effect of YQHX on Platelet Activation in Patients with IHF

To assess the impact of YQHX on platelet function and the coagulation-anticoagulation balance in patients with IHF, we measured the levels of PGI2, TXA2, and TAT. Compared to the HP control group, PGI2 levels in IHF patients were significantly lower, but they significantly increased following YQHX treatment ($P < 0.01$, Figure 5C). In line with these results, YQHX treatment significantly reversed the levels of TXA2 and TAT, causing a marked decrease ($P < 0.05$, Figure 5D and E).

## Effect of YQHX on Inflammatory Factors in Patients with IHF

To study the inflammatory response, we measured the levels of classic inflammatory cytokines TNF-α, IL-1β, and IL-6. Compared to the HP group, IHF patients had significantly higher levels of TNF-α, IL-1β, and IL-6, indicating an inflammatory burden in IHF patients. After YQHX treatment, the levels of IL-1β and IL-6 significantly decreased ($P < 0.05$, Figure 5F and G), while TNF-α showed a decreasing trend ($P > 0.05$, Figure 5H).

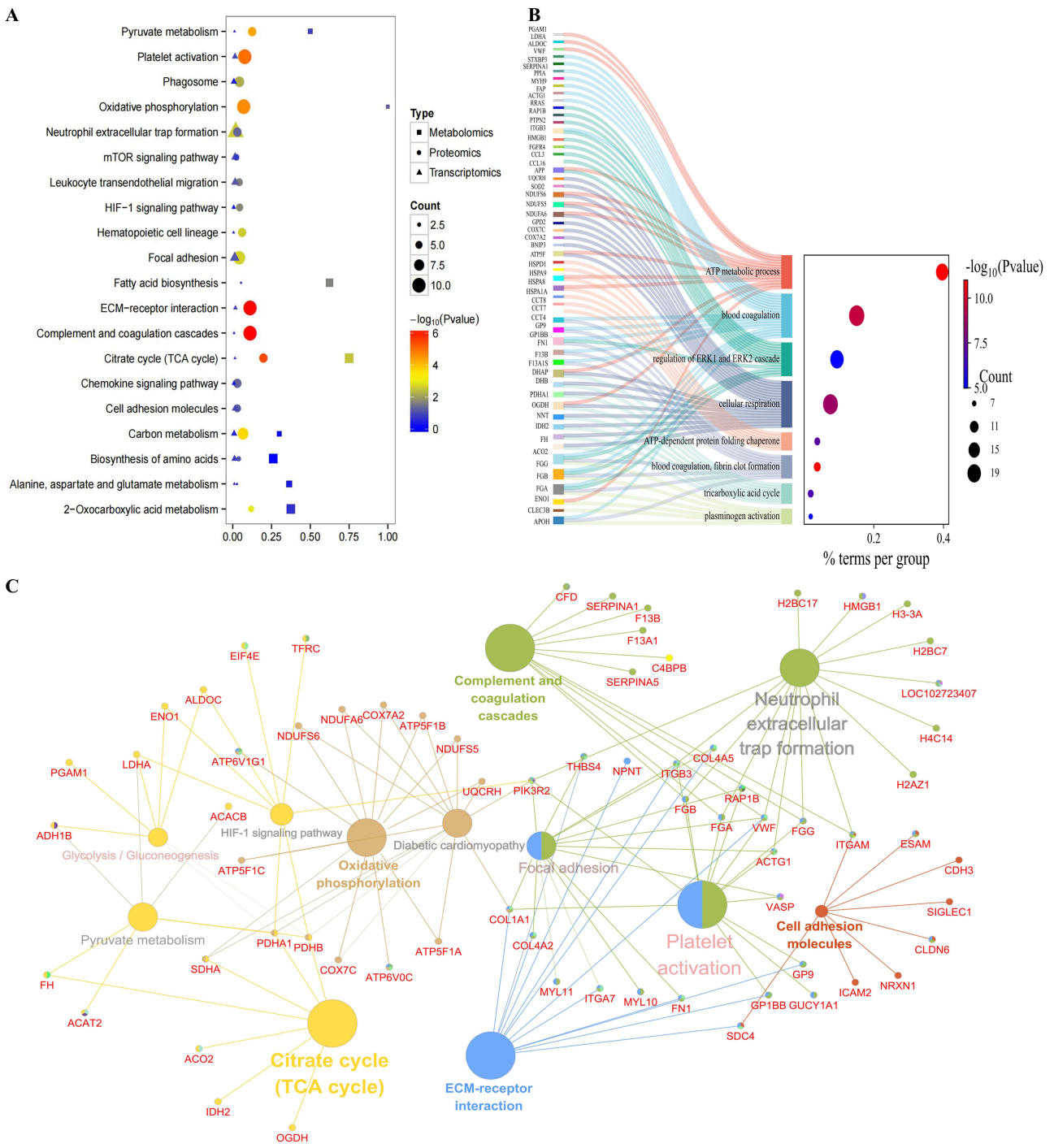


**Figure 4** Integrated analysis of multi-omics experiments. (**A**) Enrichment analysis of KEGG pathway shared by DEGs, DEPs, and DMs. (**B**) ClueGO analysis of KEGG pathway enrichment. (**C**) ClueGO analysis of GO enrichment.

## Effect of YQHX on Markers of Neutrophil Extracellular Traps (NETs) in Patients with IHF

MPO, cfDNA, Cit-H3, and NE together serve as markers of NETs. We used kits to measure the levels of MPO, cfDNA, Cit-H3, and NE in the patient samples from each group. Compared to the HP group, the levels of MPO, cfDNA, Cit-H3, and NE were significantly higher in IHF patients, indicating that excessive NET formation is closely related to the key pathological


https://doi.org/10.2147/DDDT.S525675

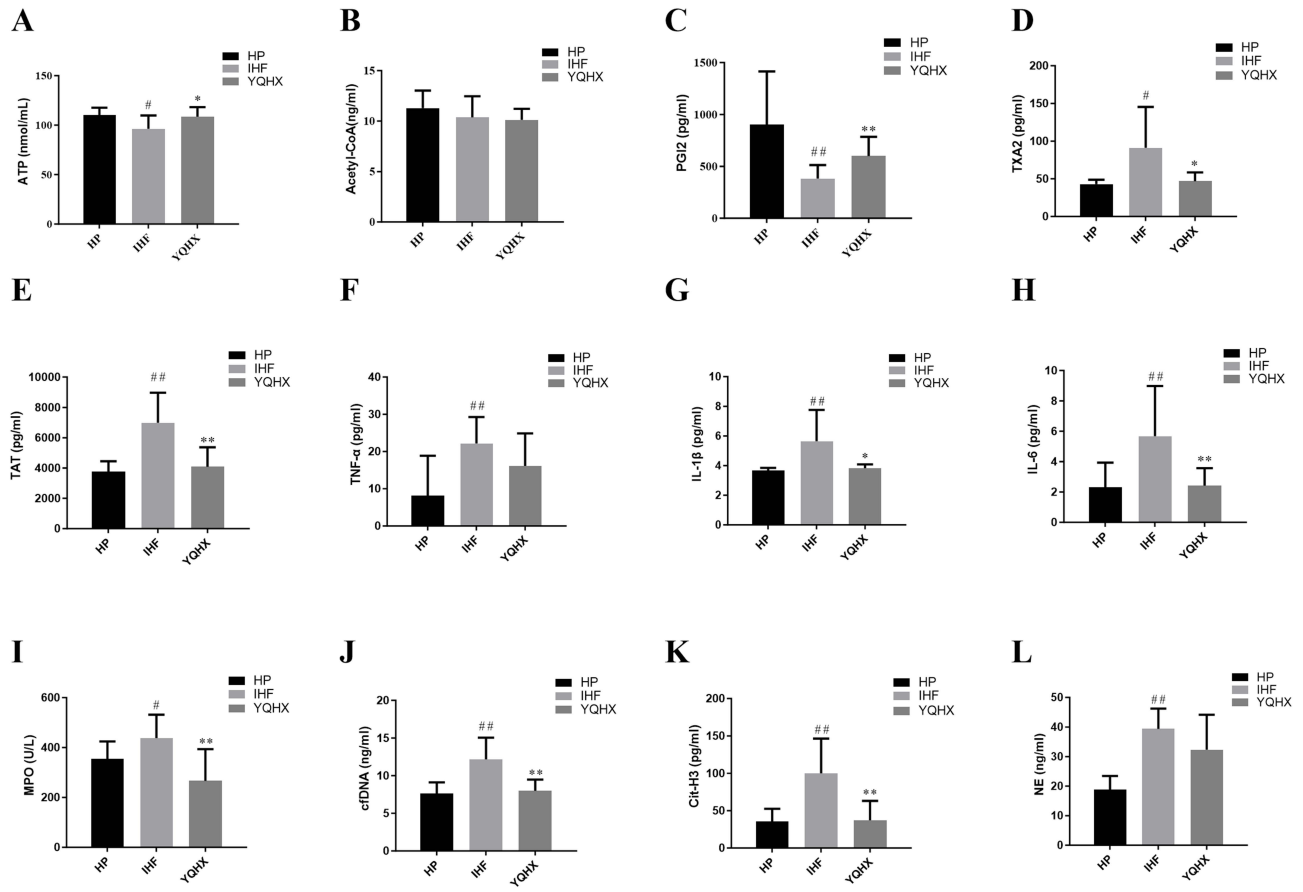


**Figure 5** Effect of YQHX on energy metabolism, platelet activation, inflammatory factors, and neutrophil extracellular traps in patients with IHF. (**A**) The level of ATP in each group. (**B**) The level of acetyl-CoA in each group. (**C**) The level of PGI2 in each group. (**D**) The level of TAT in each group. (**E**) The level of TXA2 in each group. (**F**) The level of TNF-α in each group. (**G**) The level of IL-1β in each group. (**H**) The level of IL-6 in each group. (**I**) The level of MPO in each group. (**J**) The level of cfDNA in each group. (**K**) The level of Cit-H3 in each group. (**L**) The level of NE in each group. n =10 in each group. $^{\#}P < 0.05$, $^{\#\#}P < 0.01$ vs the HP group; $^{*}P < 0.05$, $^{**}P < 0.01$ vs the IHF group.

processes of IHF. After YQHX treatment, MPO, cfDNA, and Cit-H3 levels significantly decreased ($P < 0.01$, Figure 5I–K), while NE showed a decreasing trend ($P > 0.05$, Figure 5L).

## Validation of Key Protein Targets by iPRM

To further validate key proteins from the discovery phase, iPRM-targeted proteomics was applied to verify 14 target proteins in 30 samples. A total of 13 proteins were identified as targets, with FH not being validated in the samples. Among the detected proteins, key target proteins in the platelet activation pathway, including FGA, FGB, FGG, FN1, and VWF, exhibited significant reversed upregulation. Key proteins in the energy metabolism pathway, SDHA, and IDH2, displayed significant reversed upregulation. ACO2 exhibited a trend of reversed upregulation, whereas LDHA and ENO1 showed a trend of reversed downregulation (Figure 6).

## Validation of Key Gene Targets by RT-qPCR

We further verified the expression of these identified key genes. As shown in Figure 7A–C, after YQHX treatment, most genes exhibited differential expression in IHF patients. YQHX treatment significantly suppressed the expression of ACTG1, H3-3A, and PGAM1. These genes may play a crucial role in the therapeutic effect ($P < 0.05$). After YQHX treatment, there was a trend of reduced expression of SOD2 and HMGB1, but the differences were not significant ($P > 0.05$; Figure 7D and E). Furthermore, we assessed the expression of key genes HIF-1α, mTOR, and PADI4 in the HIF-1 signaling pathway and NET formation pathway. YQHX treatment significantly suppressed the expression of HIF-1α and PADI4 ($P < 0.05$; Figure 7F and G). YQHX

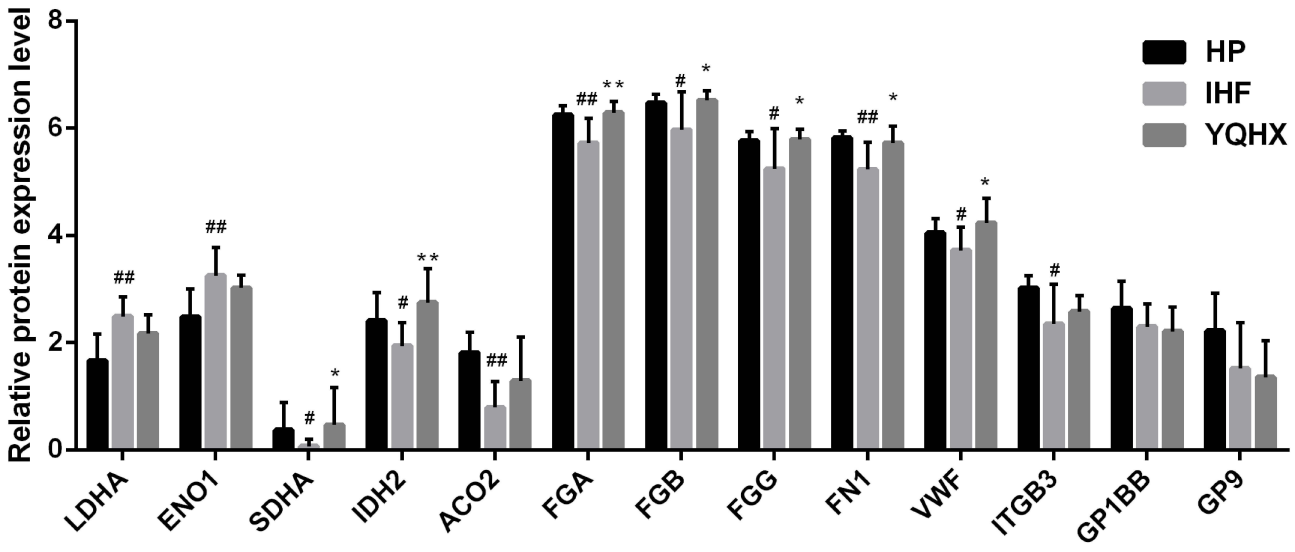


**Figure 6** Histogram of 14 target proteins verified by iPRM. Screening and validation of various differentially expressed proteins (DEPs) by PRM. n =10 in each group. $^{\#}P < 0.05$, $^{\#\#}P < 0.01$ vs the HP group; $^{*}P < 0.05$, $^{**}P < 0.01$ vs the IHF group.

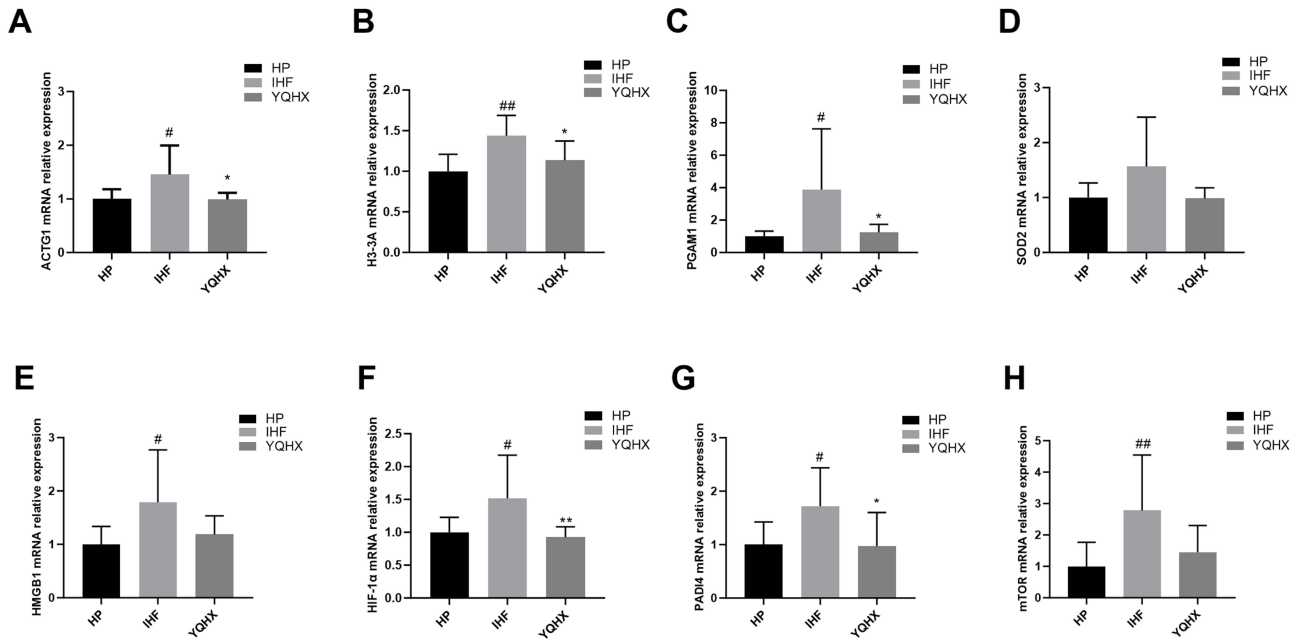


**Figure 7** RT-qPCR was conducted to determine the mRNA expression. (**A**) The mRNA expression of ACTG1. (**B**) The mRNA expression of H3-3A. (**C**) The mRNA expression of PGAM1. (**D**) The mRNA expression of SOD2. (**E**) The mRNA expression of HMGB1. (**F**) The mRNA expression of HIF-1α. (**G**) The mRNA expression of PADI4. (**H**) The mRNA expression of mTOR. n =10 in each group. $^{\#}P < 0.05$, $^{\#\#}P < 0.01$ vs the HP group; $^{*}P < 0.05$, $^{**}P < 0.01$ vs the IHF group.

treatment significantly suppressed the expression of HIF-1α and PADI4 ($P < 0.05$). The expression of mTOR exhibited a decreasing trend, but no significant statistical difference was observed ($P > 0.05$; Figure 7H).

## Molecular Docking Identified Potential Pharmaceutical Ingredients of YQHX

We profiled the chemical composition of YQHX by UPLC-Q-TOF-MS and identified 25 major bioactive compounds (Figure S1 and Table S1). Next, we performed molecular docking of all 25 identified compounds against our key targets to evaluate the affinity (also referred to as binding ability). We conducted computational virtual screening using AutoDock Vina. The virtual screening results demonstrated that astragaloside I/III/IV, isoastragaloside I/II, paeoniflorin,


https://doi.org/10.2147/DDDT.S525675

hydroxysafflor yellow A, rutin, ellagic acid, kaempferol 3-O-sophoroside, guanosine, catechin, calycosin, amygdalin, and inosine could bind to these targets, with affinities below −5 kcal/mol (Figure 8A). Figure 8B presents the representative molecular docking results of stable binding pairs between each key target and the corresponding components. Astragaloside I/III/IV, isoastragaloside I/II, paeoniflorin, and hydroxysafflor yellow A dominate the binding to key targets, exhibiting strong binding affinities.

## Effect of $CoCl_2$ on H9c2 Cells Viability

H9c2 cells survival progressively decreased in a dose-dependent manner following $CoCl_2$ exposure, with 200 μM identified as the concentration approximating the $IC_{50}$ value (Figure 9A). This concentration was consequently selected to establish the hypoxic injury model in subsequent experiments.

## The Effects of YQHX-Containing Serum and AS-IV on the Viability of H9c2 Cells

Cell viability of H9c2 cells was assessed using CCK-8 assay under varying concentrations of YQHX-containing serum (0–20%; Figure 9B). Increasing serum concentrations progressively enhanced cell viability, with the 10% group exhibiting a significant increase to 132.29% ($P<0.01$). The 10% concentration was selected as the therapeutic dose for hypoxic injury intervention due to its substantial efficacy while maintaining compatibility with standard culture conditions (10% FBS supplementation) and mitigating potential cytotoxicity risks at higher concentrations. Similarly, AS-IV treatment (5–80 μM) dose-dependently elevated cell viability (Figure 9C), where 80 μM demonstrated maximal enhancement (132.03%, $P<0.01$ vs control) and was consequently chosen for subsequent experiments based on dose-response relationships.

## YQHX-Containing Serum and AS-IV Attenuate Hypoxia-Induced Apoptosis and Inflammation in H9c2 Cells

Apoptosis rates were quantified via Annexin V-FITC/PI staining and flow cytometry. Compared to controls, hypoxia-exposed cells exhibited significantly increased apoptosis (Figure 9D and E). Both YQHX-containing serum and AS-IV treatments substantially reduced apoptosis relative to the hypoxia model group. Subsequent ELISA analysis revealed elevated production of pro-inflammatory cytokines (TNF-α, IL-1β, and IL-6) in hypoxic H9c2 cells. YQHX and AS-IV treatments effectively reversed this inflammatory response (Figure 9F–H), consistent with YQHX's anti-inflammatory effects observed clinically in IHF patients. Notably, the therapeutic efficacy of YQHX and AS-IV showed no significant difference, suggesting AS-IV as the primary bioactive component mediating YQHX's effects.

## YQHX-Containing Serum and AS-IV Ameliorate Hypoxia-Induced Impairments in ATP Content and CK Activity in H9c2 Cells

Hypoxic H9c2 cells exhibited significantly decreased ATP content and CK activity versus controls ($P < 0.01$). Both YQHX-containing serum and AS-IV treatments substantially increased ATP levels and CK activity compared to model group ($P<0.05$; Figure 9I and J), further validating YQHX's beneficial effects on energy metabolism observed in clinical samples from IHF patients.

## YQHX-Containing Serum and AS-IV Modulate Key Targets in Hypoxic H9c2 Cells

RT-qPCR analysis revealed significant upregulation of H3-3A, HMGB1, SOD2, ACTG1, and PGAM1 mRNA in model group ($P<0.01$; Figure 9K–O), consistent with clinical observations. Both YQHX-containing serum and AS-IV treatments downregulated these core target genes ($P < 0.05$), though AS-IV exerted no significant effect on H3-3A expression. Western blotting demonstrated decreased FN1 and ACO2 protein levels with elevated LDHA expression in model group. YQHX and AS-IV treatments substantially reversed these alterations, reducing LDHA while increasing FN1 and ACO2 levels (Figure 9P–S), findings compatible with competitive binding interactions predicted by molecular docking analysis.

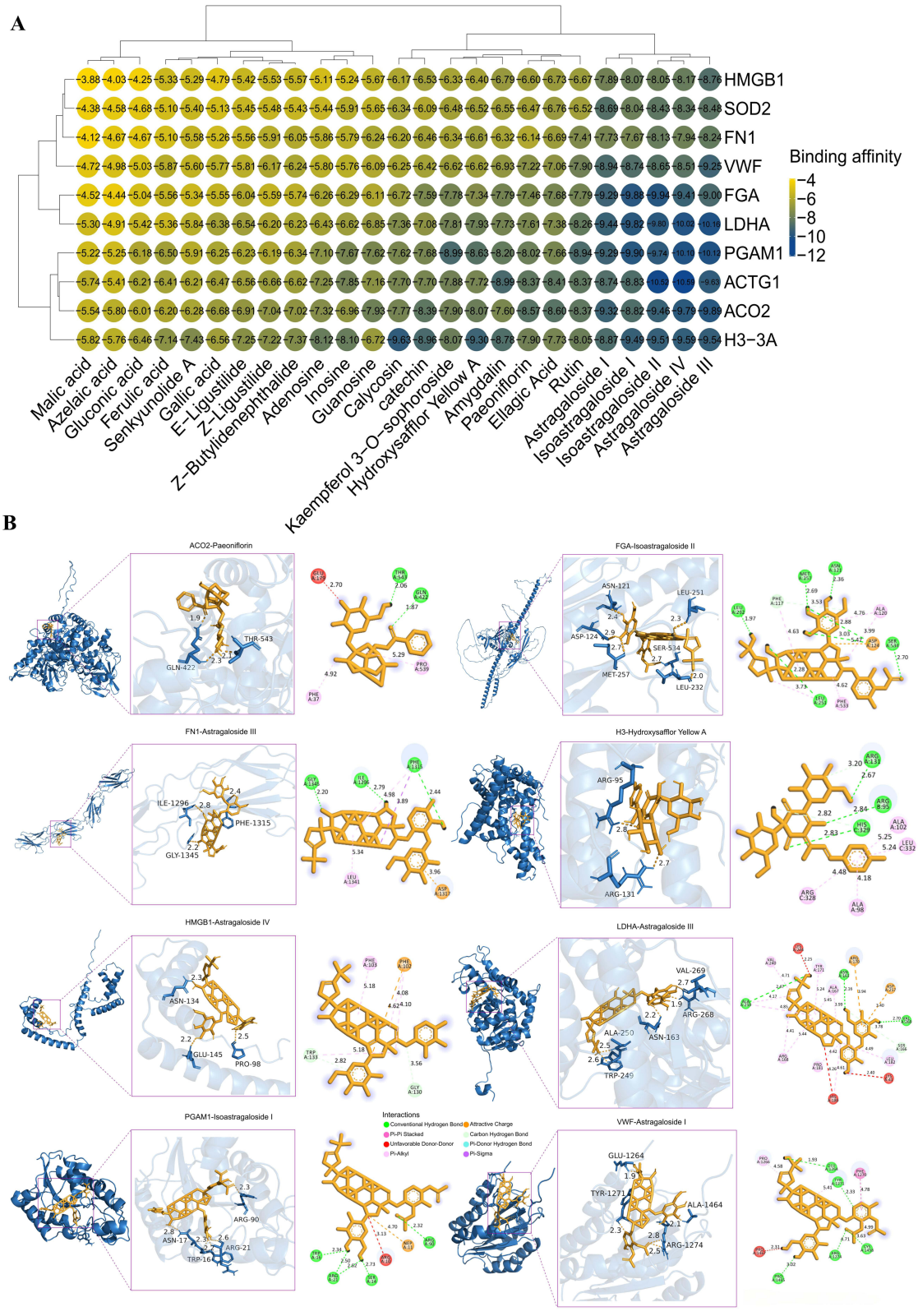


**Figure 8** Molecular docking results. (**A**) The heatmap of docking scores of key targets combining 25 active compounds in YQHX. (**B**) The representative docking complex of key targets and compounds.


https://doi.org/10.2147/DDDT.S525675

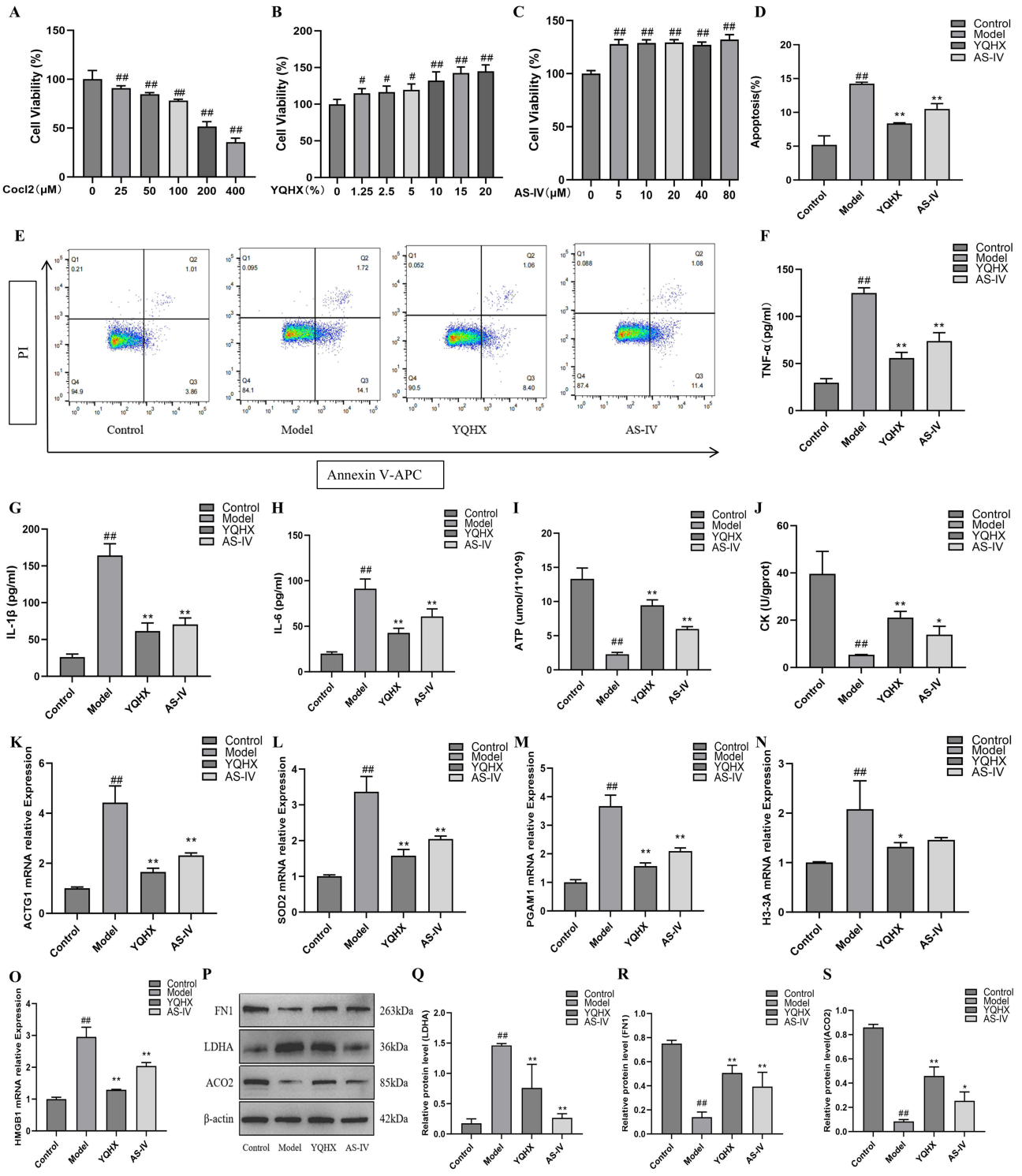


**Figure 9** In vitro experiments verified the significant effects of YQHX drug-containing serum and AS-IV in improving the hypoxia injury model of H9C2 cells. (**A**) H9c2 cells viability under varying $CoCl_2$ concentrations. (**B**) Effects of YQHX-containing serum concentrations on H9c2 viability. (**C**) AS-IV concentration-dependent effects on cell viability. (**D**) Apoptosis rates quantified by flow cytometry. (**E**) Quantitative analysis of apoptosis rates across groups. (**F**) The level of TNF-α in each group. (**G**) The level of IL-1β in each group. (**H**) The level of IL-6 in each group. (**I**) The level of ATP in each group. (**J**) The level of CK in each group. (**K**) The mRNA expression of ACTG1. (**L**) The mRNA expression of SOD2. (**M**) The mRNA expression of PGAM1. (**N**) The mRNA expression of H3-3A. (**O**) The mRNA expression of HMGB1. (**P**) Western blot analysis showed the protein expression levels of FN1, LDHA, and ACO2. (**Q**) Quantitative analysis of FN1 protein expression. (**R**) Quantitative analysis of LDHA protein expression. (**S**) Quantitative analysis of ACO2 protein expression. n = 6 in each group. $^{\#}P < 0.05$, $^{\#\#}P < 0.01$ vs the blank control group; $^{*}P < 0.05$, $^{**}P < 0.01$ vs the model group.

## Discussion

Given the effectiveness of multi-component therapies in treating complex diseases, there has been growing interest in herbal products in recent years.[19,20] YQHX, as a multi-drug formulation, has been clinically used for many years and has demonstrated good therapeutic effects on IHF in previous randomized double-blind trials.[8] To comprehensively evaluate the pharmacodynamic effects of YQHX, we initially employed the GEE model to assess its impact on cardiac function, exercise tolerance, and quality of life in IHF patients. After 12 weeks of follow-up, standard Western medical treatment combined with YQHX granules significantly reduced NT-proBNP levels in IHF patients, increased LVEF and 6MWD, and decreased MLHFQ scores, indicating that YQHX can effectively improve cardiac function, exercise tolerance, and quality of life in patients, with no severe adverse events. Subsequently, a combination of systems biology, various machine learning techniques, and molecular docking strategies was used to systematically identify the active targets and mechanisms underlying the therapeutic effects of YQHX in IHF.

While the therapeutic effectiveness of YQHX in improving IHF has been well established, its underlying molecular mechanisms and the key genes it regulates are still unknown. In this study, we performed transcriptomic, DIA proteomic, and targeted metabolomic analyses on blood samples from the HP, IHF, and YQHX groups. Venn diagram analysis revealed 31 overlapping DEGs, 62 overlapping DEPs, and 26 overlapping DMs between IHF vs HP and YQHX vs IHF, suggesting that YQHX exerts its therapeutic effects through the regulation of multiple targets, rather than a single one. To further identify the key targets, and biological pathways involved in the regulatory network of YQHX, we employed PPI network analysis combined with multiple machine learning, including LASSO, SVM-RFE, and RF. We identified H3-3A, HMGB1, SOD2, ACTG1, PGAM1, FGA, LDHA, FN1, VWF, and ACO2 as critical molecular targets in the YQHX treatment. KEGG analysis further revealed that immune response, energy metabolism, and coagulation-related pathways, including NET formation, HIF-1 signaling pathway, platelet activation, complement and coagulation cascades, TCA cycle, and glycolysis were significantly enriched. Targeted metabolomics analysis revealed the key pathways in the metabolic network regulated by YQHX, which include the citrate cycle, pyruvate metabolism, and fatty acid biosynthesis. The critical metabolites affected by YQHX treatment include citric acid, isocitrate, fumaric acid, succinic acid, L-malate, cis-aconitic acid, and L-lactic acid. To determine whether these omics layers delineate a coherent mechanistic landscape, we compared the directionality and functional enrichment of the differential markers. Although only approximately 15–20% of DEGs, and DEPs directly overlap in multi-omics studies of YQHX-treated IHF, convergence at the pathway level is markedly stronger. In our shared pathway enrichment analysis, over 50% of DEGs, DEPs, and DMs participate in the same enriched pathways—namely, platelet activation, NET formation, HIF-1 signaling pathway, TCA cycle, and glycolysis—thus underscoring robust cross-platform consistency of the core biological processes modulated by YQHX. Moreover, in IHF, markers within the HIF-1 pathway, glycolysis, and NET formation are significantly upregulated, whereas those associated with platelet activation and the TCA cycle are significantly downregulated. Notably, following YQHX treatment, these alterations are reversed. Therefore, we propose that YQHX exerts its therapeutic effects by regulating energy-metabolism reprogramming, the coagulation system, and immune-inflammatory responses (Figure 10).

In the pathological process of IHF, prolonged ischemia and hypoxia result in significant alterations in myocardial energy metabolism.[21] Our multi-omics data reveal that IHF patients exhibit metabolic reprogramming characterized by suppressed TCA cycle activity and enhanced glycolysis. This aligns with previous studies that report a shift in myocardial cells from fatty acid oxidation to glycolysis-based energy production in heart failure due to insufficient oxygen supply.[22] Notably, although this metabolic shift offers protection in the acute phase, its prolonged persistence could worsen myocardial injury. After 12 weeks of YQHX treatment, significant alterations in the metabolic pattern were observed. At both the transcriptomic and proteomic levels, YQHX significantly reduced the expression of HIF-1α and its downstream target genes LDHA, PGAM1, and ENO1, while upregulating the expression of key TCA cycle enzymes SDHA, IDH2, and ACO2. This suggests that YQHX may promote the shift of myocardial cells from glycolysis dependence to oxidative phosphorylation by inhibiting excessive activation of the HIF-1 pathway. HIF-1α plays a central role in regulating this metabolic reprogramming process. Wu et al demonstrated that HIF-1α activates the transcription of genes such as GLUT1 and LDHA to promote glycolysis while inhibiting PDH activity and reducing

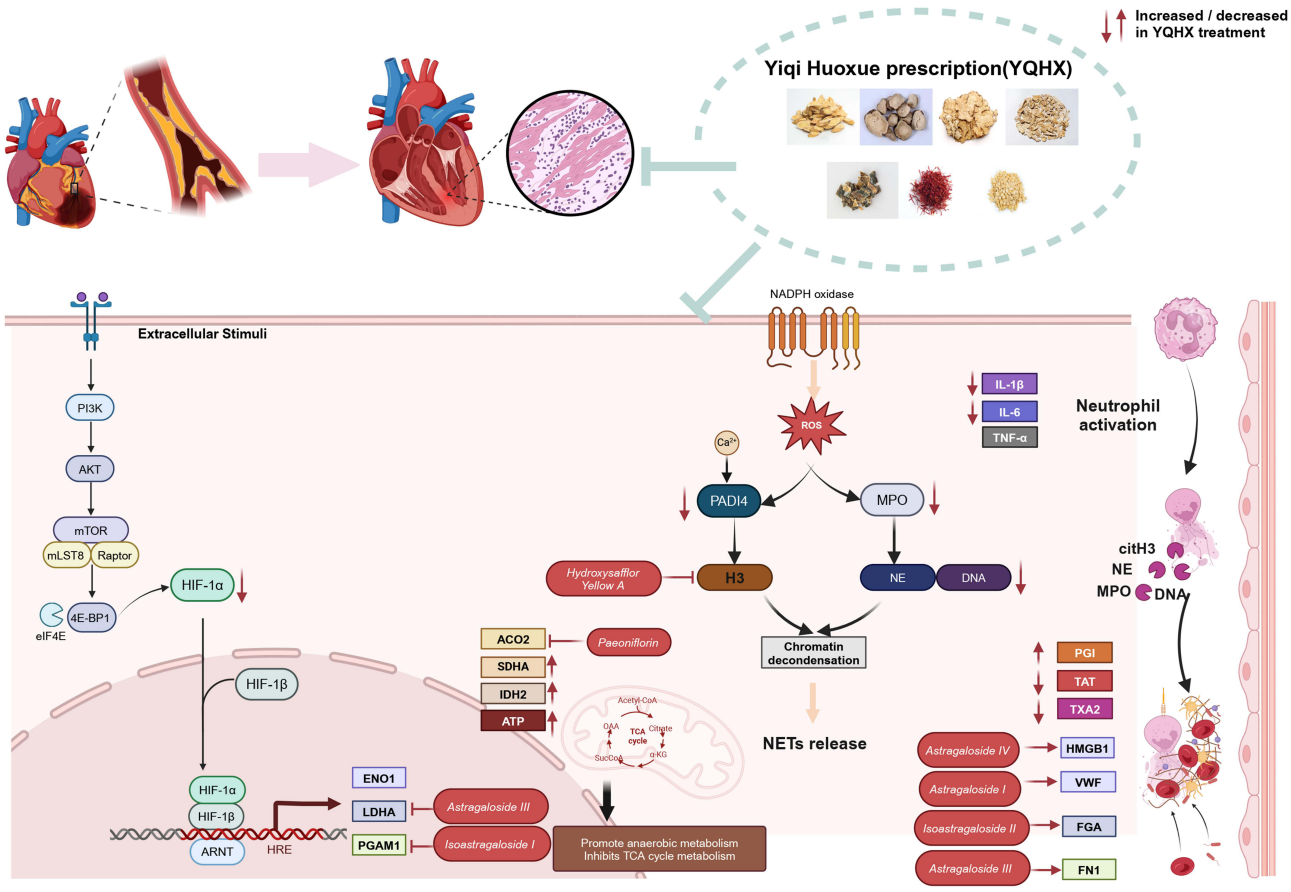


**Figure 10** Possible mechanism of the cardioprotective effects of YQHX on IHF. Upward arrows (↑) indicate activation or upregulation; downward arrows (↓) represent inhibition or downregulation.

pyruvate entry into the TCA cycle, thereby reshaping cellular metabolism under hypoxic conditions.[23] Our results indicate that YQHX treatment reduced HIF-1α expression and downregulated its downstream target genes, thereby improving abnormal metabolic reprogramming. This hypothesis is further supported by the metabolomic data. After YQHX treatment, the levels of seven TCA cycle-related metabolites tended to normalize. Notably, the reduction in lactate levels suggests that YQHX may improve myocardial acidosis and the local microenvironment by promoting aerobic metabolism and decreasing the accumulation of glycolytic byproducts. Taken together, by modulating the HIF-1/glycolysis/TCA axis, YQHX appears to restore balanced oxidative metabolism in IHF, which likely underpins its functional benefits.

Previous studies have indicated that thrombotic risk and coagulation-anticoagulation imbalance are key contributors to adverse outcomes in IHF.[24] Research by Wannamethee et al revealed a positive correlation between platelet activation and cardiac function, suggesting that platelet dysfunction may be involved in the pathological progression of HF.[25] Our study found that YQHX significantly improves coagulation function in IHF patients by increasing PGI2 levels and decreasing TXA2 and TAT levels. Given that an imbalance in the PGI2/TXA2 ratio is a key factor in abnormal platelet activation, YQHX may regulate this balance to inhibit excessive platelet activation. This is in line with the findings of Ilaria D'Agostino who showed that restoring the PGI2/TXA2 balance can prevent early cardiac fibrosis.[26] KEGG pathway enrichment analysis identified significant enrichment of the platelet activation and complement and coagulation cascades pathways, indicating that these are key targets of YQHX. Machine learning further prioritized FGA, FN1, and VWF—key mediators of fibrin formation, cell adhesion, and platelet bridging—as key proteins. Research by Nixue Song also confirmed that abnormal expression of these factors is linked to platelet activation and thrombosis in myocardial infarction patients.[27] More importantly, iPRM validation confirmed that YQHX regulates FGA, FGB, FGG, FN1, and

VWF to near-normal levels. Overall, YQHX may regulate coagulation function as a whole by systematically modulating the expression of proteins involved in the coagulation cascade.

Immune-inflammatory responses play a crucial role in the pathophysiological mechanisms of IHF.[28] Previous studies have shown that various inflammatory cytokines, such as TNF-α, IL-6, IL-1β, and IL-18, are significantly elevated in the plasma of heart failure patients.[29] These findings support the "cytokine hypothesis", suggesting that inflammation-mediated immune responses play a critical role in adverse myocardial remodeling. Furthermore, neutrophils, as key effector cells of innate immunity, play a crucial role in the inflammatory cascade and tissue damage in IHF. Activated neutrophils link inflammation to thrombosis by releasing NETs. Research has shown that NET formation is not only associated with IHF but also contributes to adverse cardiac remodeling and functional decline.[30] In this study, we found that YQHX treatment significantly improved the inflammatory response in IHF patients, as evidenced by the reversal of elevated IL-6 and IL-1β levels. Furthermore, multi-omics analysis revealed significant enrichment of the NETs pathway following YQHX treatment. Machine learning analysis identified key target proteins in this pathway, including H3-3A, HMGB1, ACTG1, and PADI4, and PCR validation confirmed their return to healthy control levels. Moreover, key NET markers MPO, cfDNA, and Cit-H3 were significantly reduced post-YQHX. Thus, YQHX appears to dampen harmful immune-inflammatory cascades and NET formation via a multi-targeted mechanism, contributing to its cardioprotective efficacy in IHF.

Twenty-five major compounds were identified through UPLC-Q-TOF/MS. Furthermore, the interaction between the main identified ingredient and predicted targets was confirmed through molecular docking technology and subsequent in vitro experiments. According to the molecular docking results, several compounds were shown to stably bind to all the validated targets. Astragaloside I/III/IV, isoastragaloside I/II, paeoniflorin, and hydroxysafflor yellow A show strong affinity for proteins involved in energy metabolism, coagulation function, and immune-inflammatory responses, making them key compounds in YQHX treatment for IHF. Recent research has shown that astragaloside-IV alleviates HF by activating PPARα, which shifts metabolism from glycolysis to fatty acid β-oxidation.[31] After astragaloside -IV treatment, fatty acid β-oxidation, and cardiac function were significantly improved in HF mice with pressure overload. This was evidenced by reduced anaerobic glycolysis, increased oxygen consumption, and enhanced expression of PPARα and its target genes, including MCPT1, MCAD, and SERCA2a.[32] Isoastragaloside I acts through the activation of the Nrf2-mediated antioxidant defense system to exert anti-inflammatory and antioxidant effects.[33] Paeoniflorin alleviates inflammation-related damage and improves cardiac dysfunction by modulating the PI3K/AKT signaling pathway and regulating levels of inflammatory cytokines such as IL-1β, IL-6, IL-12, MCP-1, and IFN-γ.[34] Additionally, Paeoniflorin has been shown to inhibit cardiac remodeling and reduce myocardial infarction and ischemia-reperfusion injury by regulating glucose and lipid metabolism, as well as through its anti-inflammatory and antioxidant effects.[35] Hydroxysafflor yellow A, identified as the major component of Carthami Flos extract, was reported by Feng et al to significantly improve cardiac function in a rat model of post-myocardial infarction heart failure, attenuate myocardial fibrosis, and suppress cardiac autophagy by inhibiting HIF-1α-mediated ROS production.[36]

To improve the comprehensiveness and precision of the study, future research can be optimized and expanded in several key areas. First, building upon the current validation of YQHX core mechanisms through integrated multi-omics, molecular docking, and in vitro functional assays, further research should prioritize in vivo verification of key targets IHF models to establish translational relevance. Second, pharmacokinetic studies quantifying systemic exposure of AS-IV and synergistic constituents (eg, paeoniflorin) will clarify bioavailability-bioactivity relationships. Additionally, dose- and time-resolved multi-omics analyses could unveil dynamic pathway regulation—particularly in platelet-mediated NETosis, HIF-1 signaling, and energy metabolism—to decode YQHX's systems-level pharmacology. This study provides crucial data support for the molecular mechanism of TCM compound therapy for IHF, offering a reference direction for future in-depth research in related fields.

## Conclusion

In this study, we innovatively combined clinical multi-omics, machine learning, molecular docking, and experimental validation to investigate the efficacy and mechanisms of YQHX in treating IHF. We demonstrated that modulating energy metabolism reprogramming, improving the coagulation system, and regulating immune-inflammatory responses are

beneficial mechanisms underlying YQHX treatment for IHF. Platelet activation, NET formation, HIF-1 signaling pathway, the TCA cycle, pyruvate metabolism, and glycolysis are indispensable pathways in treating IHF. H3-3A, ACTG1, PGAM1, FGA, FN1, and VWF are identified as key targets of YQHX treatment. Additionally, we predicted the potential active compounds of YQHX. In conclusion, our study revealed novel targets and mechanisms of YQHX in treating IHF.

## Abbreviations

CI, confidence interval; DEGs, differentially expressed genes; DM, differentially expressed metabolites; DEPs, differentially expressed proteins; GEE, generalized estimating equation; IHF, ischemic heart failure; iPRM, Intelligent Parallel Reaction Monitoring; LASSO, Least Absolute Shrinkage and Selection Operator; LC-MS/MS, liquid chromatography-tandem mass spectrometry; LVEDD, left ventricular end-diastolic diameter; LVEDV, left ventricular end-diastolic volume; LVEF, left ventricular ejection fraction; MD, mean difference; MLHFQ, Minnesota living with heart failure questionnaire; NT-proBNP, N-terminal pro-B-type natriuretic peptide; NYHA, New York Heart Association; PCA, principal component analysis; PLS-DA, partial least squares discriminant analysis; PPI, Protein-Protein Interaction Network; RF, random forest; ROC, receiver operating characteristic; RT-qPCR, real-time quantitative polymerase chain reaction; SV, stroke volume; SVM-RFE; support vector machine recursive feature elimination; TCM, Traditional Chinese Medicine; UPLC-Q-TOF-M, ultra-performance liquid chromatography coupled with quadrupole time of flight mass spectrometry; VIP, variable importance in projection; YQHX, Yiqi Huoxue prescription; 6 MWD, 6-minute walking distance.

## Data Sharing Statement

The datasets used and analyzed during the current study are available from the corresponding author, Dr. Mingjun Zhu (email: zhumingjun317@163.com), upon reasonable request.

## Ethics Approval and Informed Consent

The study protocol and informed consent form were approved by the Ethics Committee of the First Affiliated Hospital of Henan University of Chinese Medicine (Approval No: 2021HL-178). Written informed consent was obtained from all patients prior to the collection of samples.

## Acknowledgments

The authors sincerely acknowledge Professor Mingjun Zhu for his significant support and invaluable guidance. Special thanks are extended to the patients who participated in this study, the research team at the hospital for their data collection efforts, and Beijing Novogene Technology Co., Ltd. for their support in multi-omics research.

## Author Contributions

All authors made a significant contribution to the work reported, whether that is in the conception, study design, execution, acquisition of data, analysis and interpretation, or in all these areas; participated in drafting, revising or critically reviewing the article; gave final approval of the version to be published; have agreed on the journal to which the article has been submitted; and agreed to be accountable for all aspects of the work.

## Funding

This study was supported by the National Natural Science Foundation of China (Grant No.82030120), the National Science and Technology major projects (Grant No.2024ZD0522000, 2024ZD0522001), Henan Province Science and Technology Research Project (Grant No. 252102311270, 242102310548), Henan Province Key Research and Development Project (Grant No.231111310200), Henan Province Science and Technology Research and Development Plan Joint Project (Grant No. 242301420017), Natural Science Foundation of Henan Province (Grant No. 232300421308).

## Disclosure

The authors declare that they have no competing interests in this work.

## References


1. Savarese G, Becher PM, Lund LH, Seferovic P, Rosano GMC, Coats AJS. Global burden of heart failure: a comprehensive and updated review of epidemiology. *Cardiovasc Res*. 2023;118(17):3272–3287. doi:10.1093/cvr/cvac013
2. Elgendy IY, Mahtta D, Pepine CJ. Medical therapy for heart failure caused by ischemic heart disease. *Circ Res*. 2019;124(11):1520–1535. doi:10.1161/CIRCRESAHA.118.313568
3. Groenewegen A, Rutten FH, Mosterd A, Hoes AW. Epidemiology of heart failure. *Eur J Heart Fail*. 2020;22(8):1342–1356. doi:10.1002/ejhf.1858
4. Vedin O, Lam CSP, Koh AS, et al. Significance of ischemic heart disease in patients with heart failure and preserved, midrange, and reduced ejection fraction: a nationwide cohort study. *Circ Heart Fail*. 2017;10(6). doi:10.1161/CIRCHEARTFAILURE.117.003875
5. Hao P, Jiang F, Cheng J, Ma L, Zhang Y, Zhao Y. Traditional Chinese medicine for cardiovascular disease: evidence and potential mechanisms. *J Am Coll Cardiol*. 2017;69(24):2952–2966. doi:10.1016/j.jacc.2017.04.041
6. Cheang I, Yao W, Zhou Y, et al. The traditional Chinese medicine Qiliqiangxin in heart failure with reduced ejection fraction: a randomized, double-blind, placebo-controlled trial. *Nat Med*. 2024;30(8):2295–2302. doi:10.1038/s41591-024-03169-2
7. Mao J, Zhang J, Lam CSP, et al. Qishen Yiqi dripping pills for chronic ischaemic heart failure: results of the CACT-IHF randomized clinical trial. *ESC Heart Fail*. 2020;7(6):3881–3890. doi:10.1002/ehf2.12980
8. Zhu M, Wei J, Li Y, et al. Efficacy and mechanism of Buyang Huanwu Decoction in patients with ischemic heart failure: a randomized, double-blind, placebo-controlled trial combined with proteomic analysis. *Front Pharmacol*. 2022;13:831208. doi:10.3389/fphar.2022.831208
9. Wang T, Jiang X, Ruan Y, Zhuang J, Yin Y. Based on network pharmacology and in vitro experiments to prove the effective inhibition of myocardial fibrosis by Buyang Huanwu decoction. *Bioengineered*. 2022;13(5):13767–13783. doi:10.1080/21655979.2022.2084253
10. Chen M, Zhong G, Liu M, et al. Integrating network analysis and experimental validation to reveal the mitophagy-associated mechanism of Yiqi Huoxue (YQHX) prescription in the treatment of myocardial ischemia/reperfusion injury. *Pharmacol Res*. 2023;189:106682. doi:10.1016/j.phrs.2023.106682
11. Tian F, Yi J, Liu Y, et al. Integrating network pharmacology and bioinformatics to explore and experimentally verify the regulatory effect of Buyang Huanwu decoction on glycolysis and angiogenesis after cerebral infarction. *J Ethnopharmacol*. 2024;319:117218. doi:10.1016/j.jep.2023.117218
12. Ma C, Zhao J, Zheng G, et al. Qijiao Shengbai Capsule alleviated leukopenia by interfering leukotriene pathway: integrated network study of multi-omics. *Phytomedicine*. 2024;128:155424. doi:10.1016/j.phymed.2024.155424
13. Peng J, Yang K, Tian H, et al. The mechanisms of Qizhu Tangshen formula in the treatment of diabetic kidney disease: network pharmacology, machine learning, molecular docking and experimental assessment. *Phytomedicine*. 2023;108:154525. doi:10.1016/j.phymed.2022.154525
14. Li S, He Y, Lin Z, et al. Digging more missing proteins using an enrichment approach with ProteoMiner. *J Proteome Res*. 2017;16(12):4330–4339. doi:10.1021/acs.jproteome.7b00353
15. Zhang H, Liu T, Zhang Z, et al. Integrated proteogenomic characterization of human high-grade serous ovarian cancer. *Cell*. 2016;166(3):755–765. doi:10.1016/j.cell.2016.05.069
16. Feng X, Zhang Y, Du M, et al. Identification of diagnostic biomarkers and therapeutic targets in peripheral immune landscape from coronary artery disease. *J Transl Med*. 2022;20(1):399. doi:10.1186/s12967-022-03614-1
17. Sanz H, Valim C, Vegas E, Oller JM, Reverter F. SVM-RFE: selection and visualization of the most relevant features through non-linear kernels. *BMC Bioinf*. 2018;19(1):432. doi:10.1186/s12859-018-2451-4
18. Hu J, Szymczak S. A review on longitudinal data analysis with random forest. *Brief Bioinform*. 2023;24(2):bbad002. doi:10.1093/bib/bbad002
19. Huang H, Liu Y, Shuai W, et al. Atrial tachyarrhythmia prevention by Shensong Yangxin after catheter ablation for persistent atrial fibrillation: the SS-AFRF trial. *Eur Heart J*. 2024;45(40):4305–4314. doi:10.1093/eurheartj/ehae532
20. Yang Y, Li X, Chen G, et al. Traditional Chinese medicine compound (Tongxinluo) and clinical outcomes of patients with acute myocardial infarction: the CTS-AMI randomized clinical trial. *JAMA*. 2023;330(16):1534–1545. doi:10.1001/jama.2023.19524
21. Ritterhoff J, Tian R. Metabolic mechanisms in physiological and pathological cardiac hypertrophy: new paradigms and challenges. *Nat Rev Cardiol*. 2023;20(12):812–829. doi:10.1038/s41569-023-00887-x
22. Lopaschuk GD, Karwi QG, Tian R, Wende AR, Abel ED. Cardiac energy metabolism in heart failure. *Circ Res*. 2021;128(10):1487–1513. doi:10.1161/CIRCRESAHA.121.318241
23. Wu H, Zhao X, Hochrein SM, et al. Mitochondrial dysfunction promotes the transition of precursor to terminally exhausted T cells through HIF-1alpha-mediated glycolytic reprogramming. *Nat Commun*. 2023;14(1):6858. doi:10.1038/s41467-023-42634-3
24. Siniarski A, Gasecka A, Borovac JA, et al. Blood coagulation disorders in heart failure: from basic science to clinical perspectives. *J Card Fail*. 2023;29(4):517–526. doi:10.1016/j.cardfail.2022.12.012
25. Wannamethee SG, Whincup PH, Papacosta O, Lennon L, Lowe GD. Associations between blood coagulation markers, NT-proBNP and risk of incident heart failure in older men: The British regional heart study. *Int J Cardiol*. 2017;230:567–571. doi:10.1016/j.ijcard.2016.12.056
26. D'Agostino I, Tacconelli S, Bruno A, et al. Low-dose Aspirin prevents hypertension and cardiac fibrosis when thromboxane A2 is unrestrained. *Pharmacol Res*. 2021;170:105744. doi:10.1016/j.phrs.2021.105744
27. Song N, Lu D, Wu G, et al. Serum proteomic analysis reveals the cardioprotective effects of Shexiang Baoxin Pill and Suxiao Jiuxin Pill in a rat model of acute myocardial infarction. *J Ethnopharmacol*. 2022;293:115279. doi:10.1016/j.jep.2022.115279
28. Adamo L, Rocha-Resende C, Prabhu SD, Mann DL. Reappraising the role of inflammation in heart failure. *Nat Rev Cardiol*. 2020;17(5):269–285. doi:10.1038/s41569-019-0315-x
29. Dutka M, Bobinski R, Ulman-Wlodarz I, et al. Various aspects of inflammation in heart failure. *Heart Fail Rev*. 2020;25(3):537–548. doi:10.1007/s10741-019-09875-1
30. Dumont BL, Neagoe P-E, Charles E, et al. Low-density neutrophils and neutrophil extracellular traps (NETs) are new inflammatory players in heart failure. *Cana J Cardiol*. 2024;40(9):1524–1535. doi:10.1016/j.cjca.2024.03.018

31. Li M, Han B, Zhao H, et al. Biological active ingredients of Astragali Radix and its mechanisms in treating cardiovascular and cerebrovascular diseases. *Phytomedicine*. 2022;98:153918. doi:10.1016/j.phymed.2021.153918
32. Dong Z, Zhao P, Xu M, et al. Astragaloside IV alleviates heart failure via activating PPARalpha to switch glycolysis to fatty acid beta-oxidation. *Sci Rep*. 2017;7(1):2691. doi:10.1038/s41598-017-02360-5
33. Li H-L, Jin J-M, Yang C, et al. Isoastragaloside I suppresses LPS-induced tight junction disruption and monocyte adhesion on Bend.3 cellsviaan activating Nrf2 antioxidant defense system. *RSC Adv*. 2018;8(1):464–471. doi:10.1039/c7ra10246a
34. Zhai J, Guo Y. Paeoniflorin attenuates cardiac dysfunction in endotoxemic mice via the inhibition of nuclear factor-κB. *Biomed Pharmacother*. 2016;80:200–206. doi:10.1016/j.biopha.2016.03.032
35. Li X, Sun C, Zhang J, et al. Protective effects of paeoniflorin on cardiovascular diseases: a pharmacological and mechanistic overview. *Front Pharmacol*. 2023;14:1122969. doi:10.3389/fphar.2023.1122969
36. Feng J, Guo J, Yan J, et al. Luhong Formula and Hydroxysafflor yellow A protect cardiomyocytes by inhibiting autophagy. *Phytomedicine*. 2023;110:154636. doi:10.1016/j.phymed.2022.154636